Diyala Journal of Engineering Sciences

Journal homepage: https://djes.info/index.php/djes

ISSN: 1999-8716 (Print); 2616-6909 (Online)

Single Layer Metamaterial Superstrate for Gain Enhancement of A Microstrip Antenna Array

Surur Hassan Ali*, Ali Khalid Jassim

Department of Electrical Engineering, College of Engineering, Mustansiriyah University, Baghdad, Iraq

ARTICLE INFO

Article history:
Received February 28, 2024
Revised June 1, 2024
Accepted June 3, 2024
Available online June 5, 2024

Keywords:
Metamaterial Superstrate technique
Pentagonal microstrip patch antenna arrays
Quarter-wave transformer
X-band frequency range

ABSTRACT

This study focuses on creating and analyzing pentagonal microstrip patch antenna arrays with one, two, and three elements for use in the 10 GHz X-band range, utilizing a metamaterial (MTM) superstrate technique. The MTM superstrate, composed of open circular ring cells, is tailored for a 1×2 array with a 10×8 cell arrangement covering an area of 45×36 mm². A 1×3 array has a 14×12 cell configuration spanning 63×54 mm². Positioned beneath the radiating elements and optimized with a quarter-wave transformer for impedance matching, the superstrate significantly enhances antenna performance. The MTM superstrate alters the radiation pattern and increases the gain by approximately 2 dB, demonstrating a gain improvement of around 27% for high-gain applications in the X-band frequency range. For the 1×2 array, the gain increases from 7.52 dB to 9.58 dB, representing a 27.38% improvement, while the input reflection coefficient improves from -48.6 dB to -58.068 dB, reflecting a 19.5% enhancement. Similarly, for the 1×3 array, the gain rises from 9.69 dB to 11.6 dB, showing a 19.73% increase, and the input reflection coefficient improves from -57.46 dB to -60.64 dB, indicating a 5.54% improvement and a good radiation efficiency of about 79.11%. This work involves designing and simulating the proposed antenna arrays using the Computer Simulation Technology (CST) software.

1. Introduction

In contemporary wireless communication systems, the demand for high-performance antenna arrays is steadily increasing, driven by the need for faster data rates, broader coverage, and more reliable performance, particularly within the X-band frequency range; microstrip antenna arrays have become a prominent choice due to their compactness, low profile, compatibility with integrated circuit technologies, and ease of manufacture [1,2]. However, these antennas often face challenges in achieving optimal gain, wider bandwidth, and desired radiation characteristics, especially in environments characterized by multipath propagation, signal interference, and attenuation [3, 4].

To address these challenges, researchers have proposed several solutions, including employing dielectric superstrates above microstrip antenna arrays to enhance radiation characteristics [5],

* Corresponding Author
E-mail address: srwralswydawy@gmail.com
DOI: 10.24237/djes.2024.17211

modifying the geometry and dimensions of radiating elements to improve gain, bandwidth, and polarization [6], designing efficient feed networks to ensure proper impedance matching, control of radiation patterns, and minimization of losses [7], selecting optimal substrate materials with appropriate dielectric constants and loss tangents to enhance performance [8].

Optimizing the configuration and arrangement of antenna elements within the array to achieve desired radiation patterns, beam steering capabilities, and side lobe suppression [9], utilizing multilayer stack configurations to add functionalities such as polarization diversity, frequency selectivity, and impedance matching [10,11]; mutual coupling often deteriorates an antenna array's radiation characteristics, to mitigate this, the element separation should be at least λ/2 (from center to center) to avoid mutual coupling and grating lobes [12], techniques to reduce mutual coupling include implementing electromagnetic band gap (EBG) structures [13], applying neutralization techniques [14], integrating stub transitions into the feeding microstrip line [15], etching slots or slits into the ground to create Defected Ground Structures (DGS) [16,17].

Among these strategies, the use of metamaterial structures has gained significant attention due to their unique electromagnetic properties, which allow precise control over the propagation of electromagnetic waves. Strategically placed metamaterial substrates can significantly enhance microstrip antenna performance metrics such as gain, directivity, and bandwidth [18,19]; metamaterial superstrates represent a promising approach to improving microstrip antenna gain and radiation efficiency [20,21] by altering the electromagnetic environment above the radiating elements, these superstrates effectively enhance antenna performance.

Placing the metamaterial superstrate layer beneath the antenna array, rather than above [22], can modify how electromagnetic waves interact with the array; the interaction between the metamaterial layer and the underlying ground plane or substrate might impact the antenna's radiation pattern, impedance matching, or other characteristics, depending on the specific designs and their electromagnetic properties.

This study shows that earlier methods for improving microstrip antenna arrays did not deal with mutual coupling well enough and could not achieve high gain and efficiency in small designs. Adding metamaterial top layers with open circle rings nested inside each other makes matching gain, bandwidth, and impedance much better in closely packed arrays. Unlike traditional decoupling methods, this approach integrates metamaterial superstrates and optimizes array configuration, resulting in superior performance in X-band communication systems. This work bridges the gap by providing design strategies for high-gain, low-coupling antenna arrays suitable for modern, compact wireless communication systems.

This paper looks into how adding a metamaterial superstrate layer to microstrip antenna arrays can improve their performance, which could lead to better communication systems. Additionally, T-power dividers and mitered bends are incorporated into the design of the proposed array to optimize overall performance and achieve the desired radiation characteristics. The remainder of this paper is organized as follows: Section 2 describes the configurations of a single antenna, a 1 × 2 array, and a 1 × 3 array; Section 3 details the creation and testing of the Metamaterial Complementary Split Ring Resonator (MTM CSRR) unit cell and the extraction of its effective parameters; Section 4 discusses the MTM superstrate layer, Section 5 presents the outcomes, measurements, and simulations of the final design; and Section 6 compares these results. Finally, Section 7 concludes the paper.

2. Design of antennas

2.1. Single element antenna

Fig. 1(a and b) shows the printed pentagonal antenna shape steps. It was made on an FR-4 substrate $(25\times28)mm^2$. It had parameters (εr = 4.3, h = 1.4 mm, and tan δ = 0.025). A 50 Ω microstrip feeding line makes up the antenna. A rectangular slot is etched with a size of $(2.98\times3.62)mm^2$ on a radiating patch to enhance gain and obtain a low input reflection coefficient.

The final input reflection coefficient of the antenna is lowered to -67.781 dB at a resonance frequency of 10 GHz. The single element has a good gain value of 6.07 dB. Table 1**.** shows the comparison results for the performance of the single pentagonal antenna. The simulation results for the S-parameter for each stage in the antenna design are also presented in Fig. 2. This paper focuses on the pentagonal patch shape, which is widely discussed in the literature. The pentagonal shape enables the patch to work with circular polarisation (CP) [23], obtaining phase quadrature with constant amplitude. Benefits of CP include improved penetration, increased maneuverability, and reduced susceptibility to interference. Equations (1) to (3) aim to ascertain the pentagonal patch's dimensions.

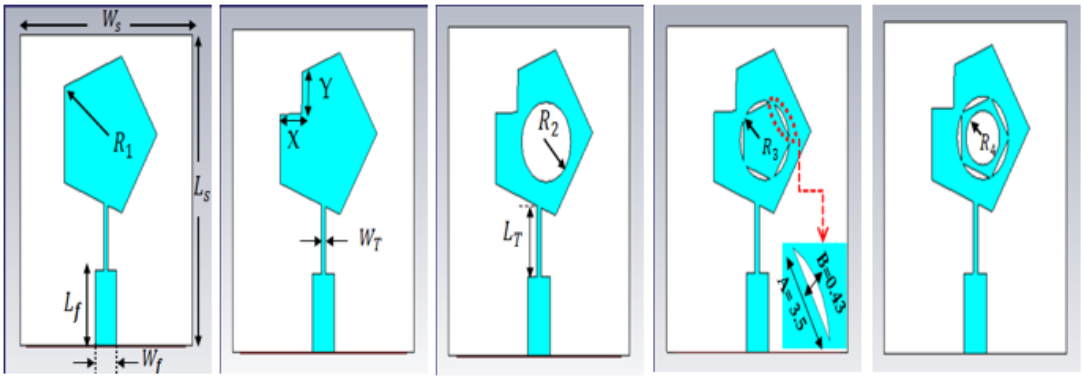

a) Top view

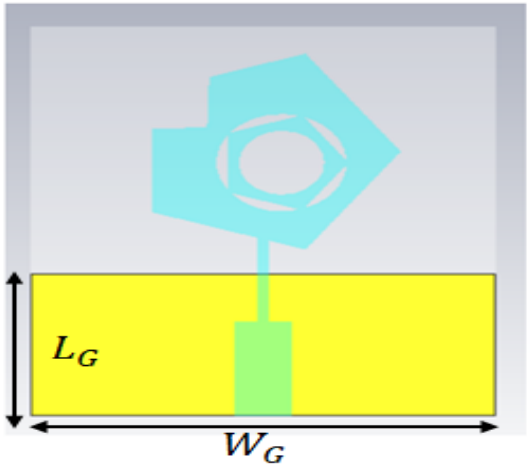

b) Bottom view

Figure 1. Evolution stages of the proposed single pentagonal antenna design (I) Stage 1;(II) Stage 2 ; (III) Stage 3 ; (VI) Stage 4 ; (VII) Stage 5 (proposed)

Table 2. displays the optimal dimensions of the single-element MPA. Where W is the width of the patch, h is the substrate thickness, fr is the resonance frequency, λ is the wavelength, and C is the vacuum speed of light. These equations are given below [24]:

$$W = \frac{C}{2f_r}\sqrt{\frac{2}{\varepsilon_r+1}} \quad (1)$$

$$\varepsilon_{reff} = \frac{\varepsilon_r+1}{2} + \frac{\varepsilon_r-1}{2}\left[1+12\frac{h}{w}\right]^{-\frac{1}{2}} \quad (2)$$

$$\lambda = \frac{C}{f_{r\times}\sqrt{\varepsilon_{eff}}} \quad (3)$$

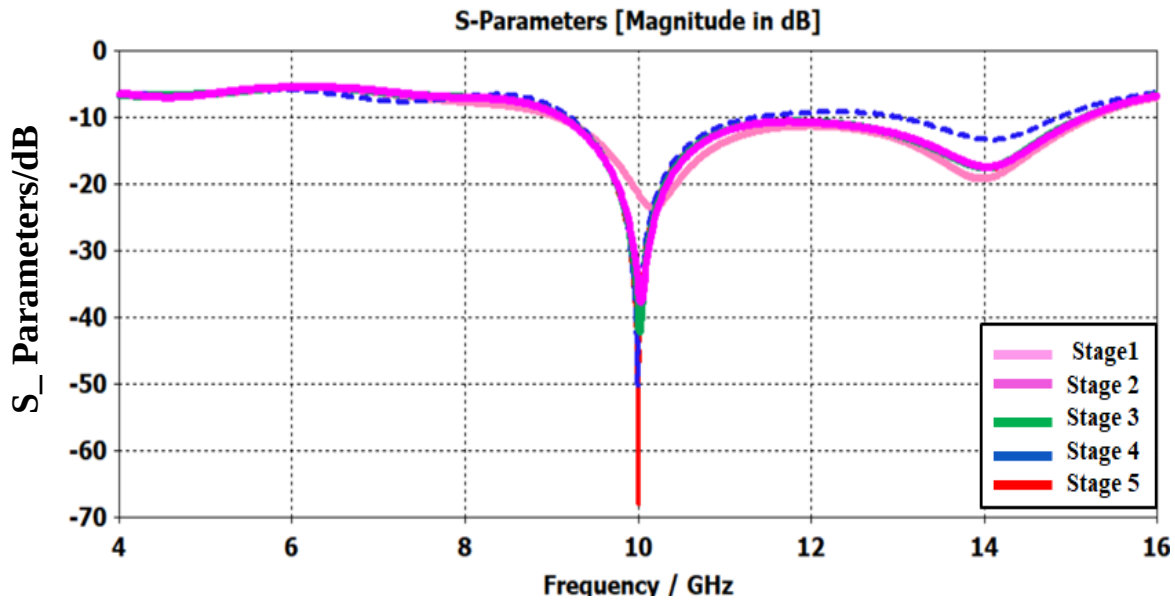

Figure 2. S-parameter simulation for each design stage

Table 1: Comparative results of the proposed single-element microstrip patch antenna's performance

Geometry	Bandwidth (MHz)	Working Freq. (GHz)	Return losses (dB)	Gain (dBi)
Stage 1	(9.07-15.22)GHz 6152.2 MHz	10.18 GHz	-23.5	5.24
Stage 2	(9.13-15.17)GHz 6036 MHz	10.036 GHz	-37.77	5.99
Stage 3	(9.13-15.17)GHz 5623 MHz	10 GHz	-50.08	5.96
Stage 4	(9.22-11.36)GHz 2143 MHz	10 GHz	-42.24	6.01
Stage5 Proposed	(9.13-15.15)GHz 6016 MHz	10 GHz	-67.78	6.07

Table 2: The optimal dimensions of the single element MPA

Symbol	Value (mm)	Symbol	Value (mm)	Symbol	Value (mm)
R_1	7.4	L_G	10.27	Y	3.62
W_f	3.1	W_S	25	R_2	3.4
L_f	6.8	L_S	28	R_3	3.6
W_T	0.6	H	1.4	R_4	2.3
L_T	6	t	0.035	A	3.51
W_g	25	X	2.98	B	0.43

Designing a microstrip antenna array requires the combination of multiple antenna elements to achieve constructive interference in a desired direction, thereby enhancing the overall gain. Achieving optimal performance in terms of coverage, gain, directivity, efficiency, radiation pattern, and beam steering capabilities necessitates careful consideration of several factors:

1. Arrangement of Array Elements: The physical configuration of the array elements (e.g., linear, planar, or circular) significantly

influences the coverage and beam steering capabilities of the antenna.

2. Spacing Between Array Elements: The separation between adjacent array elements plays a crucial role in determining the radiation pattern and beamwidth of the array antenna. Although smaller spacing generally leads to higher directivity and narrower main lobes, it can also increase mutual coupling between elements. Mutual coupling is the interaction between adjacent elements, potentially altering their performance. Conversely, larger spacing can reduce mutual coupling but may broaden the main lobe and increase side lobe levels.
3. Phase Control of Array Elements: The design of a microstrip antenna array is not just about the physical configuration but also about the advanced technology that enables precise phase adjustment of each element relative to its neighbors. This precision allows the radiation pattern and beam direction to be steered electronically without physically moving the antenna. This exact phase control, a testament to advanced technology, makes beamforming possible by directing the main lobe towards a particular angle or point of interest.
4. Transmission Line Feed: The transmission line feed network distributes RF signals from the antenna feed point to individual array elements. Proper design of this network is essential to ensure impedance matching, phase synchronization, and appropriate power distribution. These factors are further discussed in Section 2.2.

2.2. 1×2 Antenna Array

Figure 3(a and b) showcases the geometrical layout of a two-element conventional microstrip patch antenna array designed for operation at a frequency of 10 GHz. The array is constructed on an FR-4 substrate measuring 38.5×34.1mm^2. The T-junction power divider [25] has a significant quarter-wavelength dependence on the output port. With a 50 Ω input impedance, this port plays a crucial role in ensuring the proper excitation of the proposed antenna array and adequate power distribution to each element. The optimal dimensions for a 1×2 element MPA array are outlined in Table 3.

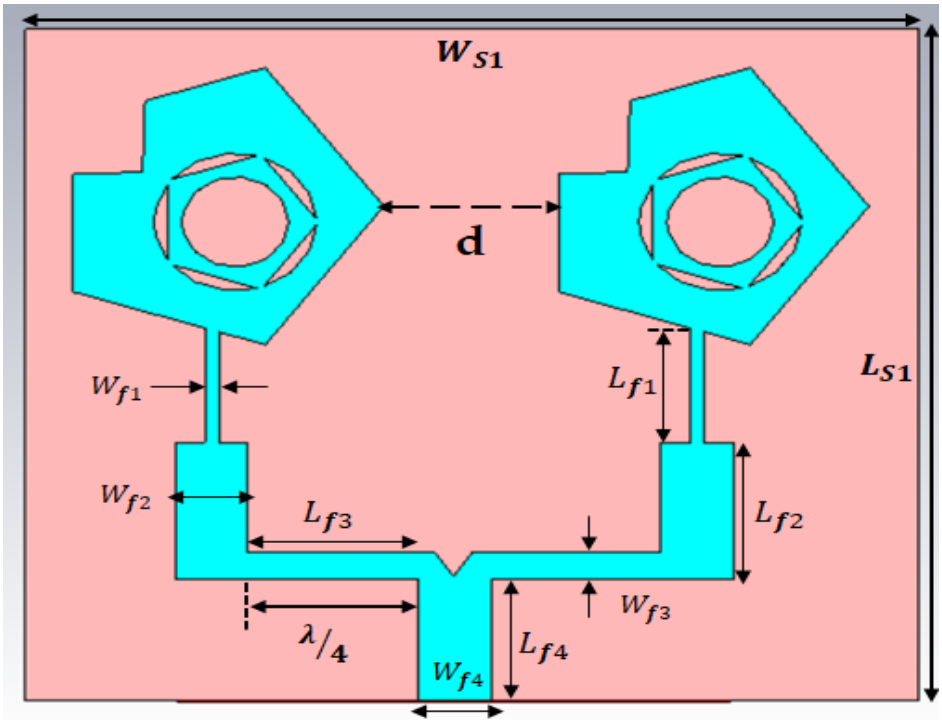

a) Front view

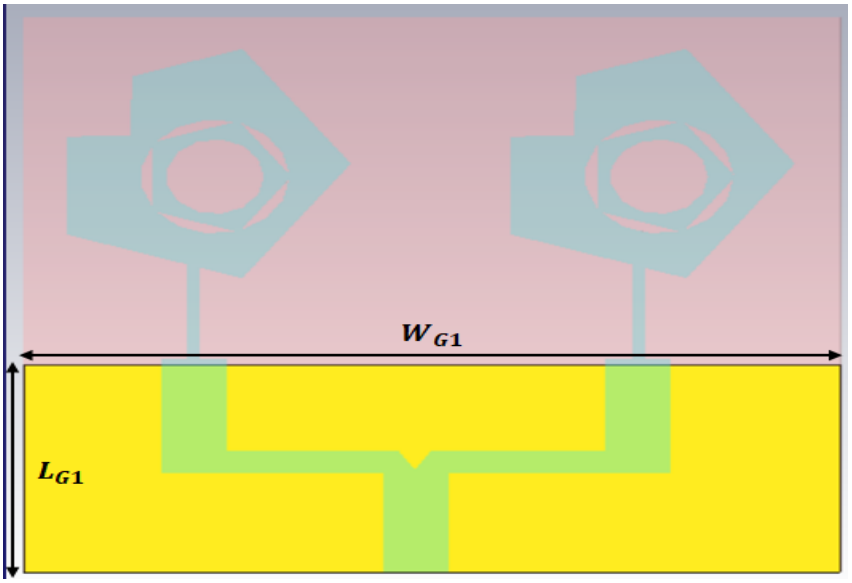

b) Back view

Figure 3. Schematic diagram of cooperate-fed 1 × 2 antenna array

Table 3 : The optimal dimensions of 1 × 2 element MPA array

Substrate		**Ground**	
W_{S1}	38.5 mm	W_{G1}	38.5 mm
L_{S1}	34.1 mm	L_{G1}	12.78 mm
Z_a = 50 Ω feedline		Z_b = 100 Ω feedline	
W_{f2}	2.75 mm	W_{f1}	0.63 mm
L_{f2}	7 mm	L_{f1}	5.8 mm
W_{f4}	2.75 mm	Z_c = 70.7 Ω feedline	
L_{f4}	6.1 mm	W_{f3}	1.44 mm
Spacing between patches	7.5 mm	L_{f3}	7.35m

It is often necessary to employ optimization techniques based on simulation results to achieve optimal performance from antenna equipment and meet specific parameters. Components such as cut slots or curved feed mechanisms play significant roles in determining the antenna's radiation characteristics and ensuring effective power distribution to each patch. The incorporation of a triangular cut slot represents a modification to the conventional design, as depicted in Fig. 3. These will be designed as follows:

The spacing between array elements: From edge to edge, the distance between array elements should be about a quarter of the wavelength (λ/4) to minimize mutual coupling, prevent single-mode propagation among radiating elements due to random errors, and ensure that array elements are in phase with each other and radiate in the normal direction [26].

Thus, $\lambda_{air} = \frac{C}{f_r} = \frac{3 \times 10^8}{10 \times 10^9} = 30\ mm,$

Patch spacing (from edge to edge), d= $\frac{\lambda_{air}}{4} = \frac{30}{4} = 7.5\ mm$. So, a parametric study was done using a parameter sweep for different separation distances between two elements of MPA arrays until the best results were found at the best distance. It was found that a distance of 7.5 mm gave the best return losses and gain values of -48.6 dB and 7.52 dB, respectively. Fig. 4. shows the return losses of linear antenna arrays as a function of the spacing between elements. The results are shown in Table 4 below:

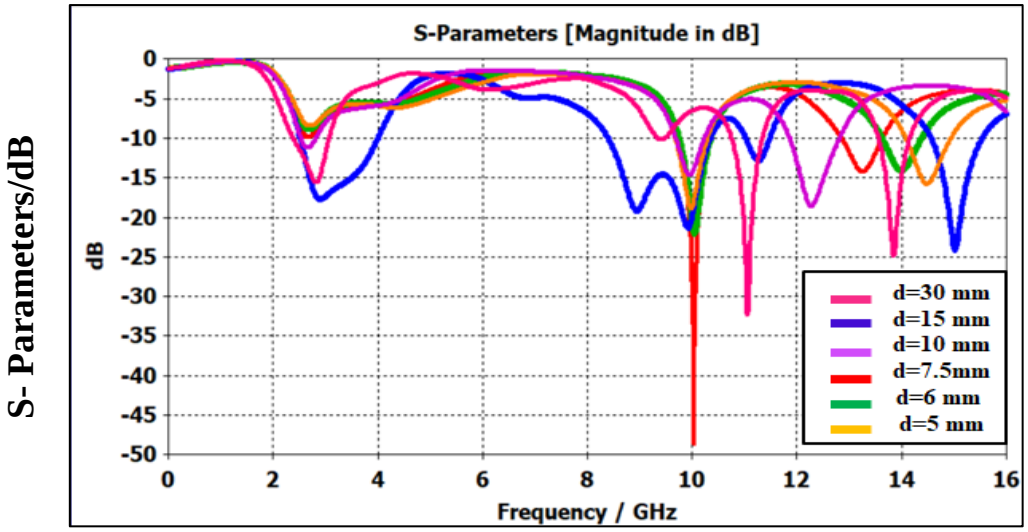

Figure 4. The return losses of linear antenna arrays are a function of spacing between elements

Table 4: Return losses & gain between antenna arrays for different separations

d (mm)	s_{11} (dB)	Gain(dB)
λ (30 mm)	-32.317	4.86
$\lambda/_2$ (15 mm)	-21.2	4.43
$\lambda/_3$ (10 mm)	-14.32	7.14
$\lambda/_4$ (7.5 mm)	-48.6	7.52
$\lambda/_5$ (6 mm)	-22	7.57
$\lambda/_6$ (5 mm)	-18.84	7.5

- **Transmission Line Feeding:** The T-power divider network is a crucial component for effective power distribution among array members, ensuring that each element in the array receives the necessary power. as depicted in Figure 5. This feeding network has three branches: 50 Ω, 100 Ω, and 70.7 Ω. In a parallel array feed network for the proposed antenna, a microstrip-feed line of (Z_a = 50 Ω) branches off into two feed lines of $2Z_a$ (Z_b= 2×50 =100 Ω), which further ramose into a Z_C = 70.7 Ω feed line as indicated (4) [27].

$$Z_C = \sqrt{Z_a Z_b} \quad (4)$$

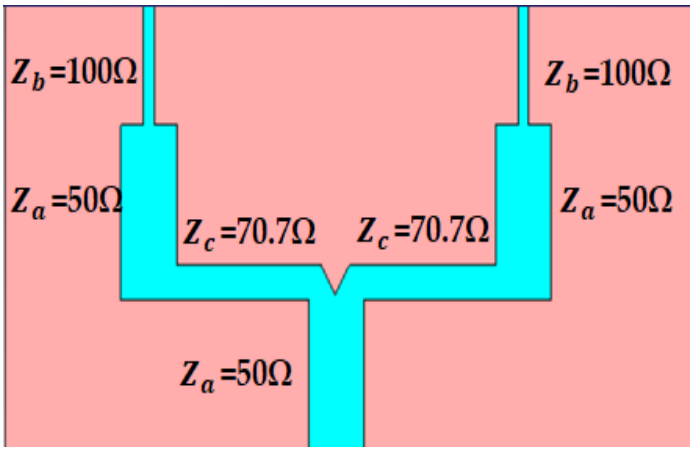

Figure 5. T-junctions configuration of the proposed power divider

The characteristic impedances mostly depend on the power divider's width and the separation between the divider and the ground plane. The impedance of the feedline width (2.75 mm, 0.63 mm, and 1.44 mm) for 50Ω, 100Ω, and 70.7Ω, respectively, is determined by matching each element of the array to the standard 50 Ω impedance. The following equations (5–7) were used to compute the supply of the feedline width for each impedance [27]:

$$A=\frac{Z_0}{60}\sqrt{\frac{\varepsilon_r+1}{2}}+\frac{\varepsilon_r-1}{\varepsilon_r+1}\left(0.23+\frac{0.11}{\varepsilon_r}\right) \quad (5)$$

$$B=\frac{377\pi}{2Z_0\sqrt{\varepsilon_r}} \quad (6)$$

$$W_f=\begin{cases}\frac{8he^A}{e^{2A}-2} & ,for\ \frac{W_f}{h}\le 2\\ \frac{2h}{\pi}\left[B-1-\ln\left((2B-1)+\left(\frac{\varepsilon_r-1}{2\varepsilon_r}\right)\left\{\ln(B-1)+0.39-\frac{0.61}{\varepsilon_r}\right\}\right)\right] & ,for\ \frac{W_f}{h}\ge 2\end{cases} \quad (7)$$

The feed line width of $Z_a = 50\ \Omega$ was calculated as follows:

$$A=\frac{50}{60}\sqrt{\frac{4.3+1}{2}}+\frac{4.3-1}{4.3+1}\left(0.23+\frac{0.11}{4.3}\right)=1.51,$$

$$W_f=\frac{8\times1.4\times e^{1.53}}{e^{2(1.53)}-2}=2.75\ \text{mm}.$$

The feed line width of $Z_b = 100\ \Omega$ was calculated as follows:

$$A=\frac{100}{60}\sqrt{\frac{4.3+1}{2}}+\frac{4.3-1}{4.3+1}\left(0.23+\frac{0.11}{4.3}\right)=2.87,$$

$$W_f=\frac{8\times1.4\times e^{2.87}}{e^{2(2.87)}-2}=0.63\ \text{mm}.$$

The feed line width of $Z_c = 70.7\Omega$ was calculated as follows:

$$A=\frac{70.7}{60}\sqrt{\frac{4.3+1}{2}}+\frac{4.3-1}{4.3+1}\left(0.23+\frac{0.11}{4.3}\right)=2.077,$$

$$W_f=\frac{8\times1.4\times e^{2.077}}{e^{2(2.077)}-2}=1.44\ \text{mm}.$$

2.3. 1×3 Antenna Array

The previous 1×2 configuration can be expanded by adding another radiating element to create a 1×3 antenna array. One can achieve this expansion by altering the feeding network or using a T-power divider to distribute signals to each component evenly. The spacing between the elements is 7.5 mm, equivalent to 0.25 λ0 at a frequency of 10 GHz. The CST simulator's parameter sweep optimization (PSO) tool has been utilized in multiple optimizations attempts to achieve impedance matching, lower return losses, and good gain characteristics. The total size of the 1×3 array design is (59.05 × 48.3) mm². Table 5 shows the optimal dimensions of the 1×3-element microstrip patch antenna (MPA) array. Figure 6 illustrates the geometry of a conventional three-element array with corporate feeding at 10 GHz.

Table 5: The optimal dimensions of 1 x 3 element MPA array

Substrate		**Ground**	
W_{S2}	59.05 mm	W_{G2}	59.05 mm
L_{S2}	48.3 mm	L_{G2}	32.63 mm
Z_a = 100 Ω feedline		Z_b = 50 Ω feedline	
W_{f4}	0.63 mm	W_{f6}	2.75 mm
L_{f4}	10.8 mm	L_{f6}	9.5 mm
W_{f4}	0.63 mm	Z_c = 70.7 Ω feedline	
L_{f4}	9.2 mm	W_{f3}	1.44 mm
Spacing between patches	7.5 mm	L_{f3}	17.8mm

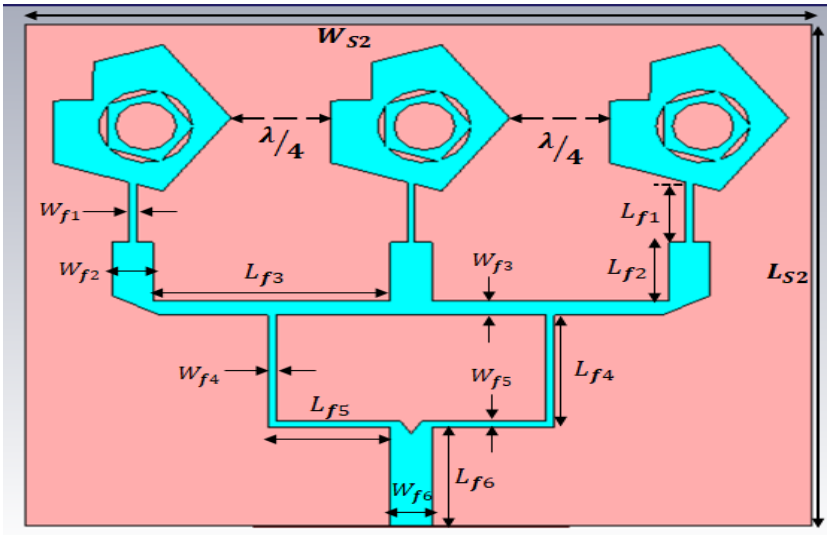

a) Front View

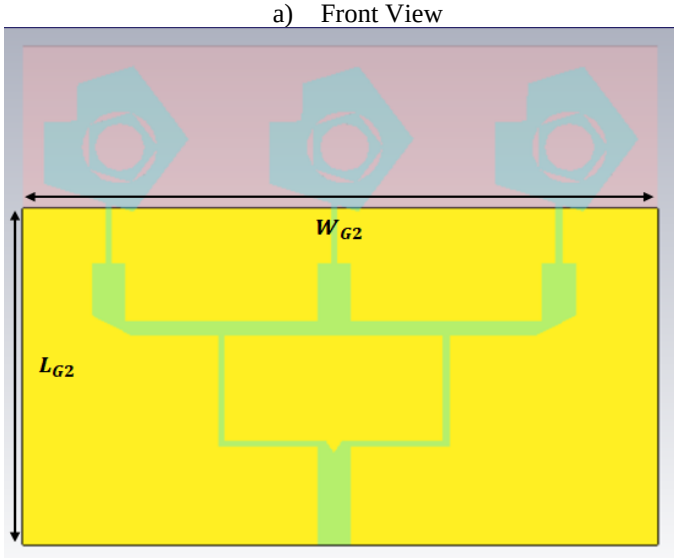

b) Back View

Figure 6. Schematic Diagram of Cooperate-fed 1 × 3 antenna array

Transmission Line Feeding: We have modified the conventional design 1×3 array using the curved feeding method called "mitered bend," as illustrated in Figure. 7. It is a technique used to create bends in transmission lines. Instead of a traditional curved bend, the ends of the transmission lines are cut at a certain angle; the cutting angle is often calculated through electromagnetic simulations or experimentation to achieve the best performance for the particular array antenna design. This method of cutting helps lower issues like VSWR (Voltage Standing Wave Ratio), insertion loss (loss of signal power when parts are connected), and return loss (power being reflected to the source). These issues can worsen in line bends, where most of the energy from the input is sent back to the source when the line is cut [28]. This, in turn, leads to a mismatch with the input port resistance, which reduces system performance. The primary function of the curved feed in the antenna is to facilitate radiation and reduce return losses. They ensure sufficient power distribution to each radiating patch. Meanwhile, mitered bends help preserve signal integrity and compactness within the array structure.

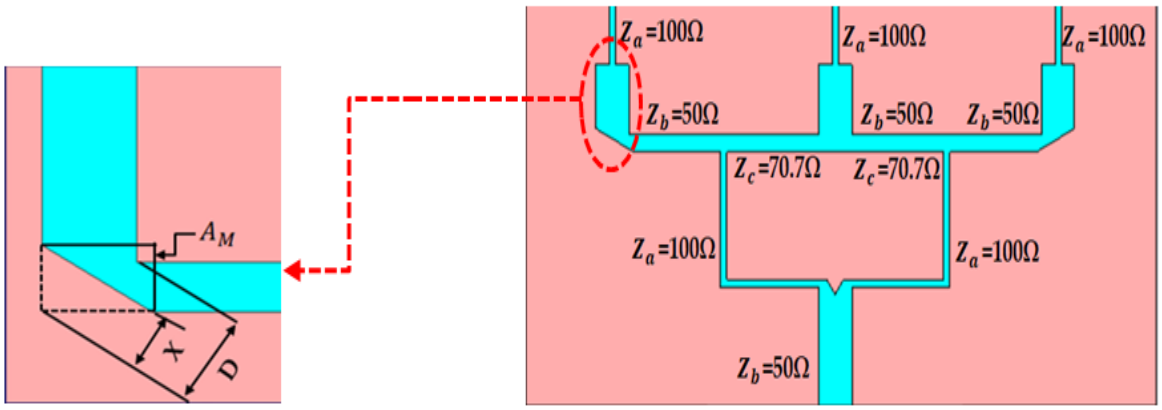

Microstrip Mitred Bend

Fig. 7. The proposed power divider

Microstrip Mitred Bend Calculator: The feeding network of the antenna array design will only include the bend at $Wf3$ = 1.44 mm in the input impedance 70.7 Ω line. where A_M= compensated length for optimal bend, D = square mitre's diagonal, h = substrate height, and W_f = transmission line width. Equations 8 to 10 provide expressions for X, D, and AM as follows [29]:

$$D = W_f \times \sqrt{2} \quad (8)$$

$$= 1.44 \times \sqrt{2} = 2.03 \text{ mm}$$

$$X = D \times \left[0.52 + 0.65e^{(-1.35 \times \frac{W_f}{h})}\right] \quad (9)$$

$$= 2.03 \times \left[0.52 + 0.65\, e^{(-1.35 \times \frac{1.44}{1.4})}\right]$$

$$= 1.4 \text{ mm}$$

$$A_M = (X - \frac{D}{2}) \times \sqrt{2} \quad (10)$$

$$= (1.4 - \frac{2.03}{2}) \times \sqrt{2} \quad = 0.51 \text{ mm}$$

The simulations show that connecting three antennas created four separate frequency bands at 2.81 GHz, 6.01 GHz, 10 GHz, and 13.96 GHz. These bands gave simulated results (for |S11| < -10 dB). At 10 GHz, the simulated gain, directivity, and input reflection coefficient achieve 9.7 dBi, 12.4 dBi, and -57.46 dB, respectively. Figure 8 (a , b) illustrates the input reflection coefficient characteristics with gain versus frequency of a three-element array.

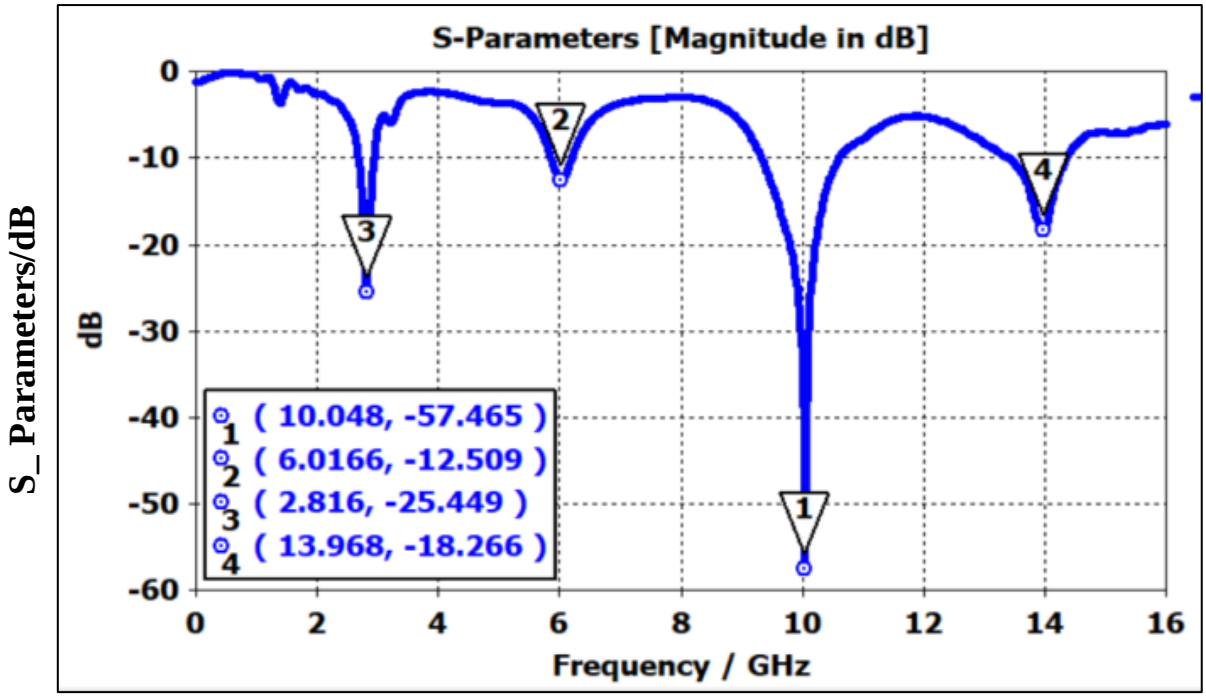

a)

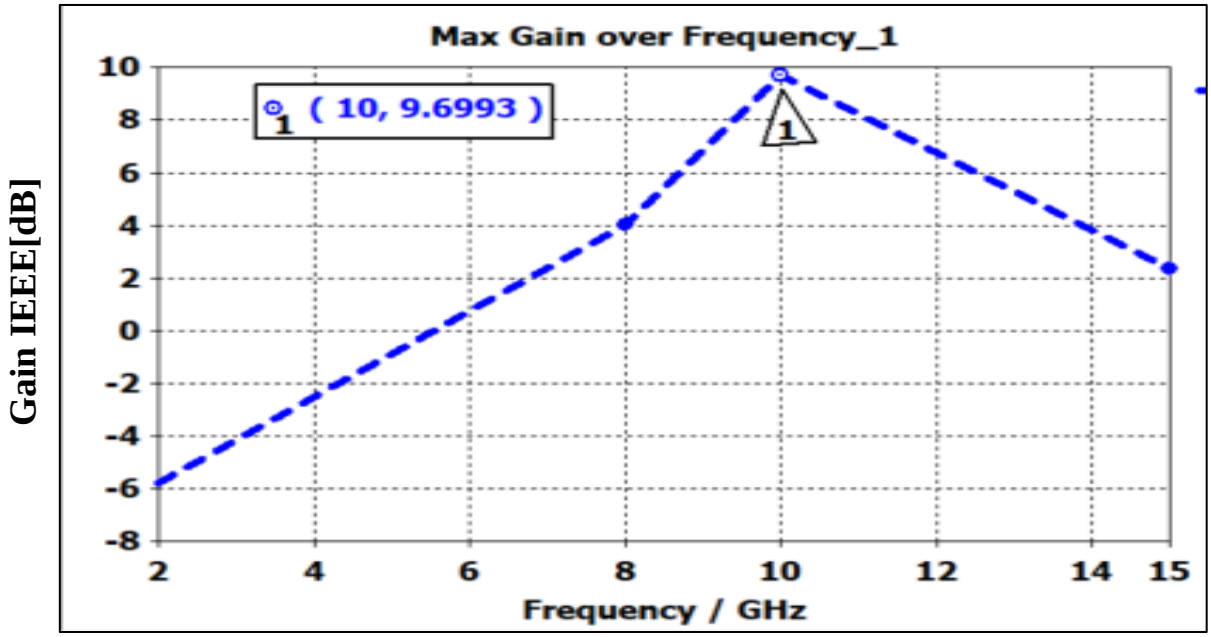

b)

Figure 8. a) The S-parameter characteristics VS frequency of a three-element array **b)** The gain VS frequency of a three-element array

3. Design of metamaterial unit cell

The CSRR unit cell configuration and its built-in equivalent circuit are shown in Figure 9 (a, b). The structure is carefully placed between two waveguide ports in the ±x direction, with an electromagnetic wave and magnetic and electric fields running along the y- and x-axes, respectively. This suggests that the first port sends the reflecting signal while the second receives the receiving signal. The C-shaped double CSRR unit cell size is optimized and simulated to determine the effective behavior of the S11 reflection phase of the proposed unit cell

and the negative electromagnetic properties at 10.1 GHz, as shown in Figure 10(a,b). The suggested CSRR unit cell's geometric measurements are shown in Table 6.

Table 6: The CSRR-MTM unit cell dimensions

Symbol	R_1	R_2	W_x	L_x	g1	g2	b1
Value (mm)	1.34	0.85	4.5	4.5	0.25	0.25	0.27

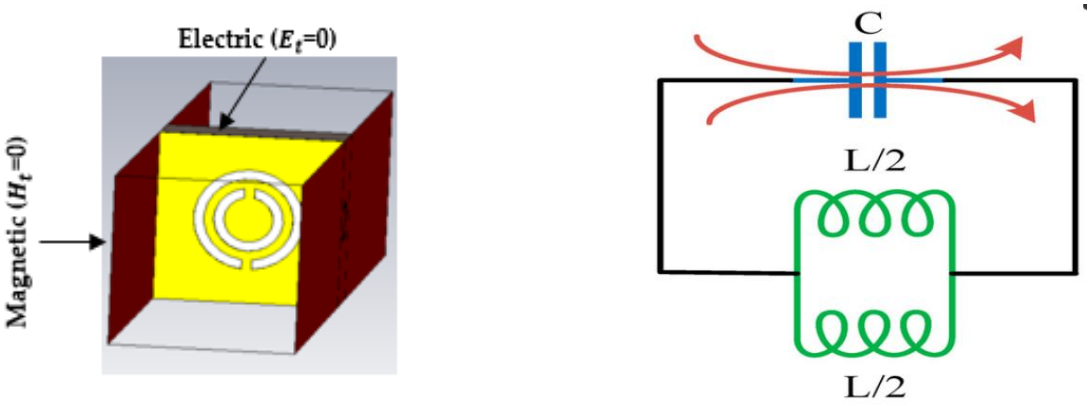

a) b)

Figure 9. a) A 3-D perspective view of the unit cell. b) The equivalent circuit of the unit cell

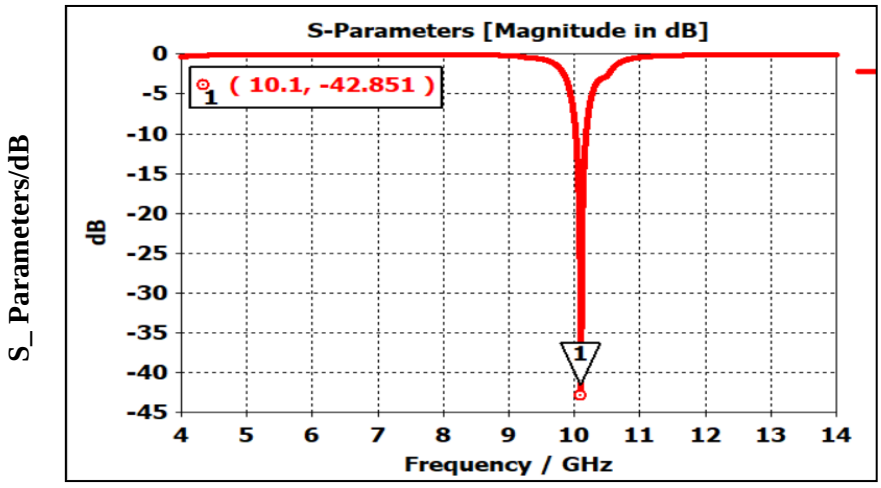

a)

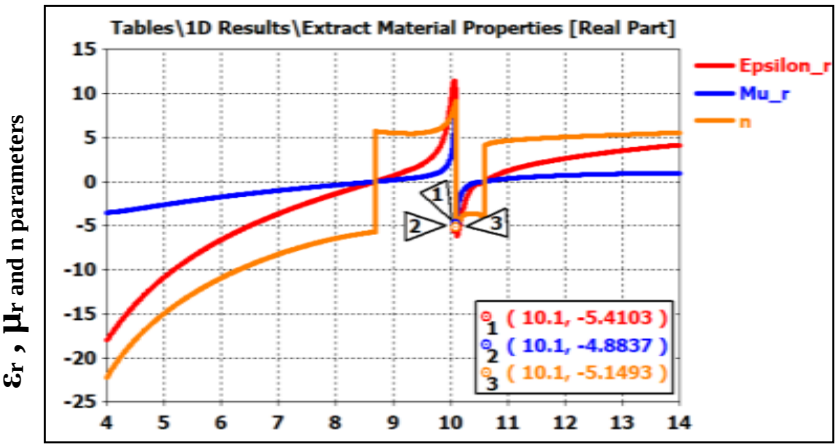

b)

Figure10. (a) (S_{11}) of the metamaterial unit cell; (b) $\mathcal{E}_{eff}$; μ_{eff} ; n parameters

4. Metamaterial superstrate layer analysis for gain enhancement

The antenna's gain can be increased by putting different-sized MTM superstrate layers below the suggested antenna array with two and three elements. This is possible because the MTM superstrate layer uniquely reflects surface waves outside the resonance range, raising the antenna array's gain. The metamaterial superstrate layer can be engineered to reflect waves and focus or steer them in the desired directions. Additionally, metamaterials can manipulate the phase and polarization of reflected waves, offering further flexibility in controlling the behavior of the electromagnetic field.

The proposed MTM cells are printed above the FR-4 substrate (εr = 4.3, h = 1.4 mm, and $tan\delta$=0.025). One layer of copper with a thickness of 0.035 mm is added. Two open circular resonators are etched, one imbricated inside the other, on the top of the substrate, while a complete ground is not added on the back. For the 1×2 antenna array approach, the MTM superstrate layer has a total area of (45×36) mm^2 and consists of a (10×8) cell array. For the 1×3 antenna array approach, the MTM superstrate layer has a total area of (63×54) mm^2 and consists of a (14×12) cell array, as shown in Figures 11 and 12. The geometry of the MTM superstrate covers the proposed antenna array with two or three elements. The fabricated photo of the (10 × 8) array MTM superstrate layer is shown in Figure 13.

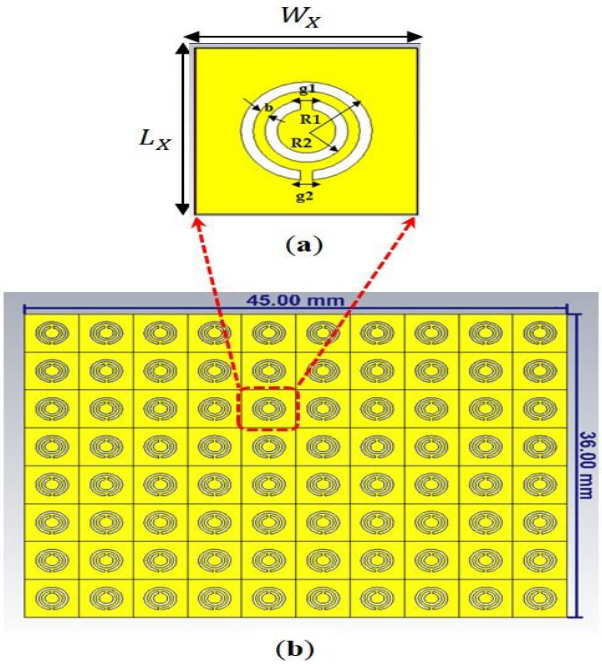

Figure 11. The geometry of the MTM superstrate: (a) Unit Cell SRR and (b) (10 × 8) array Unit Cell SRR–based 1×2 MPA arrays

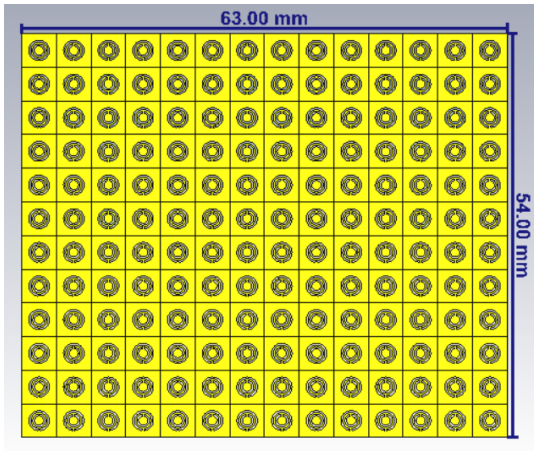

Figure 12. The geometry of the MTM superstrate for (12 × 14) array Unit Cell SRR-based 1×3 MPA arrays

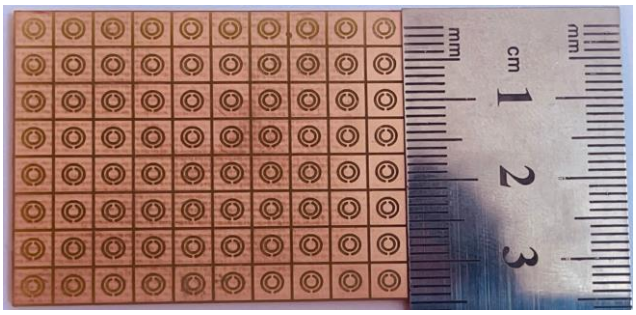

Figure 13. The fabricated structure of the (10 × 8) MTM superstrate layer array cell

5. The Results and discussion

5.1. Gain and reflection coefficient (S11) results

A single layer of metamaterial substrate is incorporated into the design of the proposed antenna array, which sits below the 1 × 2 and 1 × 3 antenna arrays covered in Sections 2 and 4, respectively. This integration aims to enhance gain and minimize back radiation. Several parametric studies, as described below, have been carried out to optimize gain and return loss characteristics:

1. A parametric study of the antenna peak gain reveals that the gain increases with the number of cells, as indicated in Table 7. The size of the MTM superstrate layer affects the radiation behavior of the antenna, as shown in Figures 11 and 12. The benefit gained may be sacrificed in favor of a smaller MTM superstrate layer, as illustrated in Figure 14.

Table 7: The gain value for various numbers of unit cells for 1×2 array

No. of cells	Gain (dB)
10×8	9.58
10×7	9.08
10×6	8.93
9×6	8.74

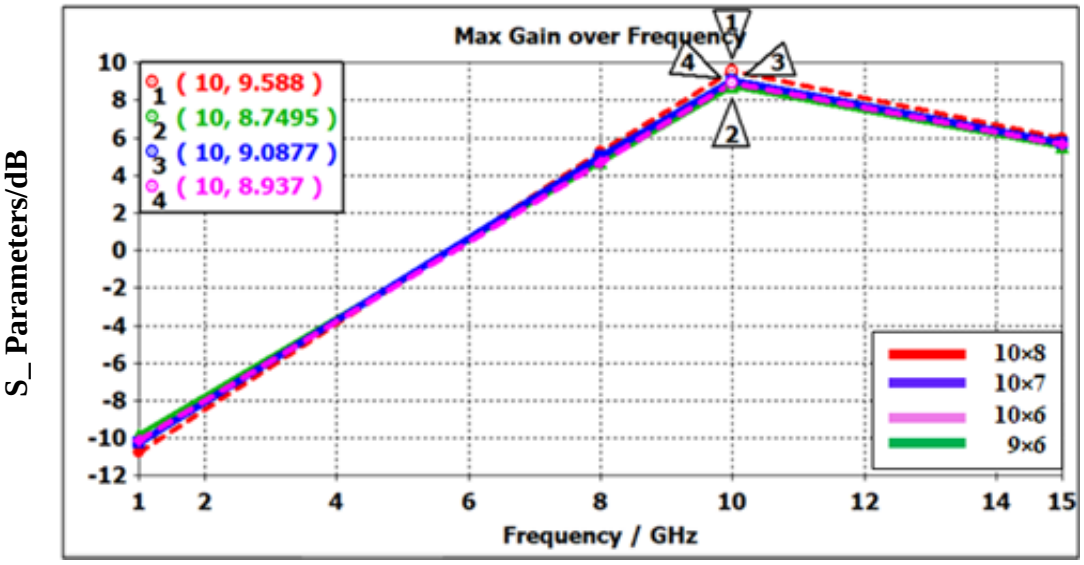

Figure 14. Gain parametric analysis for various numbers of unit cells for a 1×2 array

2. Another important parametric study focused on the spacing (S) between the proposed array antenna and the MTM superstrate layer, as shown in Figures 15(a) and 16(a). This parameter is crucial to optimizing the antenna's radiation characteristics. As anticipated, the MTM layer has a significant impact on the antenna array's peak gain and return losses, as seen below:

A- For 1×2 element array approach:

Figure 15 (b and c) illustrates the fluctuations in the input reflection coefficient and the gain value at a frequency of 10 GHz. The input reflection coefficient drops to -58.068 dB as the spacing (S) increases and reaches the distance S = 14.2 mm. The impact of this parameter on the radiation characteristics is shown in Table 8, where the peak gain of the array antenna increases to 9.58 dB at a distance of S = 10 mm.

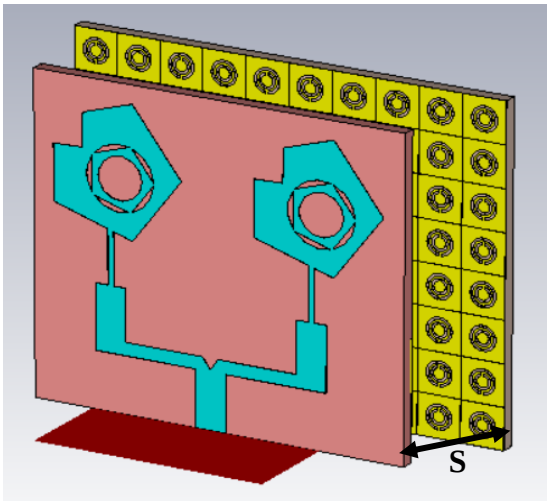

a)

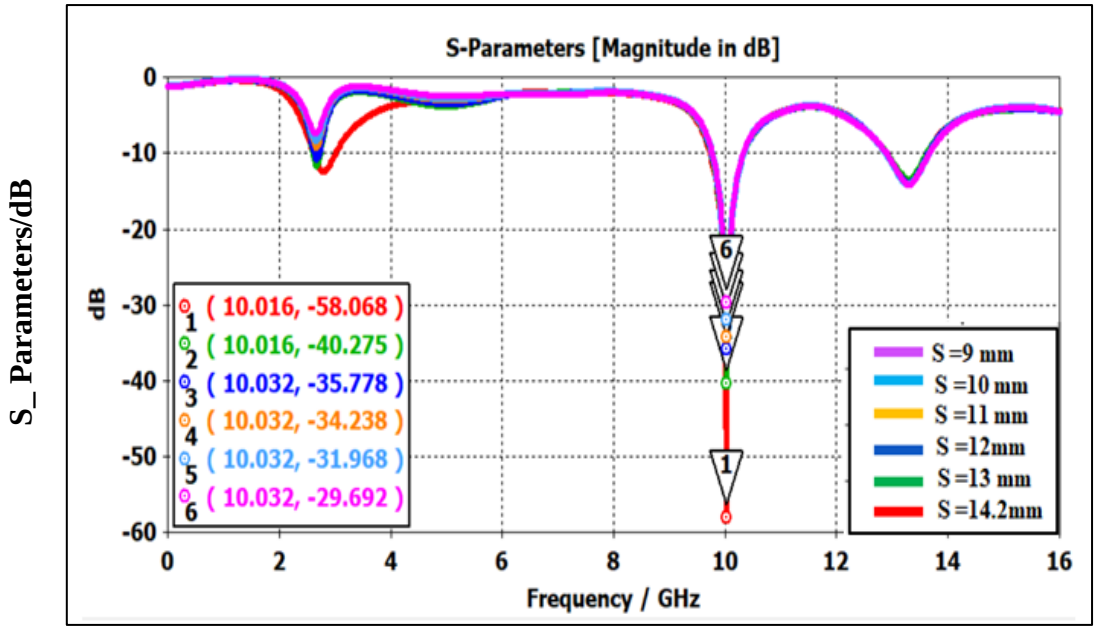

b)

Figure 15. a) Perspective view of the embedded 1×2 antenna array with MTM Superstrate layer **b)** Analysis of S11 parameters at various distances at 10 GHz

Table 8: Return losses & gain of 1×2 antenna array with the reflector for different spacing

Spacing between 1×2 antenna array and MTM superstrate layer (S)mm	Input reflection coefficient S_{11}(dB)	Gain (dBi)
9	-29.69	9.24
10	-31.96	9.588
11	-34.23	9.24
12	-35.77	9.12
13	-40.27	8.998
14.2	-58.068	8.79

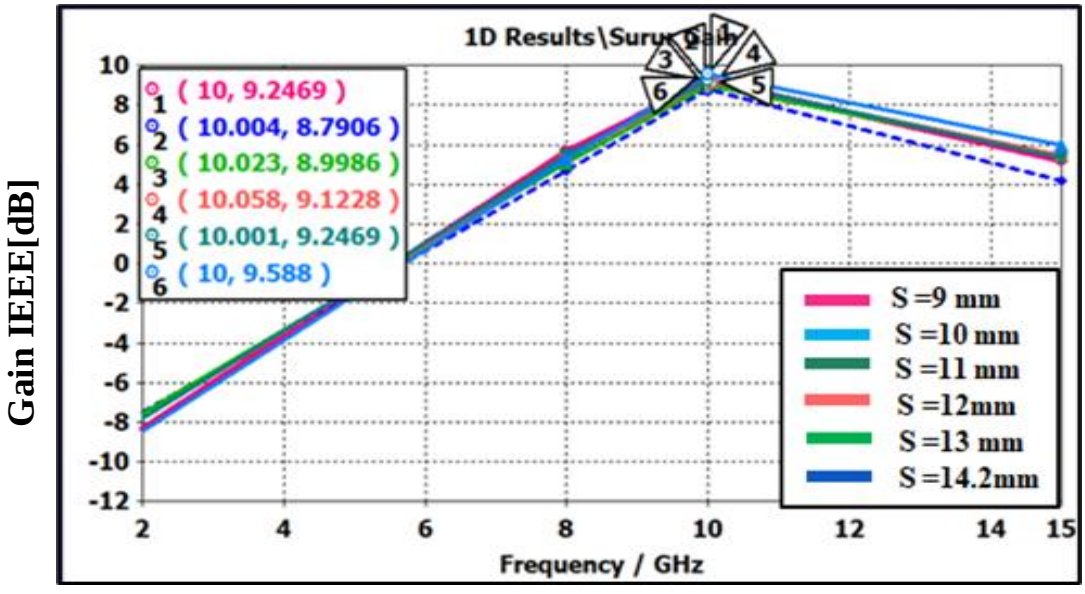

Figure 15. c) The gain parametrically at different distances at 10 GHz

B- For 1×3 element array approach

Figure 16 (b and c) illustrates the fluctuations in the input reflection coefficient and the gain value at a frequency of 10 GHz. The input reflection coefficient drops to -60.64 dB as the spacing (S) increases and reaches the distance S = 18 mm. Table 9 shows how this parameter affects the radiation characteristics as the peak gain of the array antenna rises to 11.6 dB at a distance of S = 10 mm.

In conclusion, the operating band stays stable at the 10 GHz resonant frequency. The distance from the reflective metasurface layer affects the antenna array's highest peak gain and lowest return losses. The 1×2 element array antenna methodology produced an appropriate response to the reflection coefficient (S11) when S = 14.2 mm, equivalent to less than (λ /2), and a stable high gain when S = 10 mm. The 1×3 element array antenna methodology produced an appropriate response to the reflection coefficient (S11) when S = 18 mm and a stable high gain when S = 10 mm.

Ultimately, the performance behavior of the antenna array is demonstrated by the gain increase to 9.58 dB for two-element arrays and 11.6 dB for three-element arrays. The MTM superstrate layer is positioned above the conventional antenna array at an optimal distance. In compliance with Snell's law of refraction, electromagnetic waves are scattered from the primary source and directed along the normal of the medium by a material with a low refractive index. This property significantly enhances the directivity of the proposed antenna.

Due to the strong reflection from the MTM superstrate, the antenna exhibits exceptional performance. In this context, enhancing the stability of the proposed antenna array will further increase its overall gain. Figure 17 (a and b) compares the S11 and gain results for a single element, a 1×2 element array, and a 1×3 element array with the MTM superstrate layer.

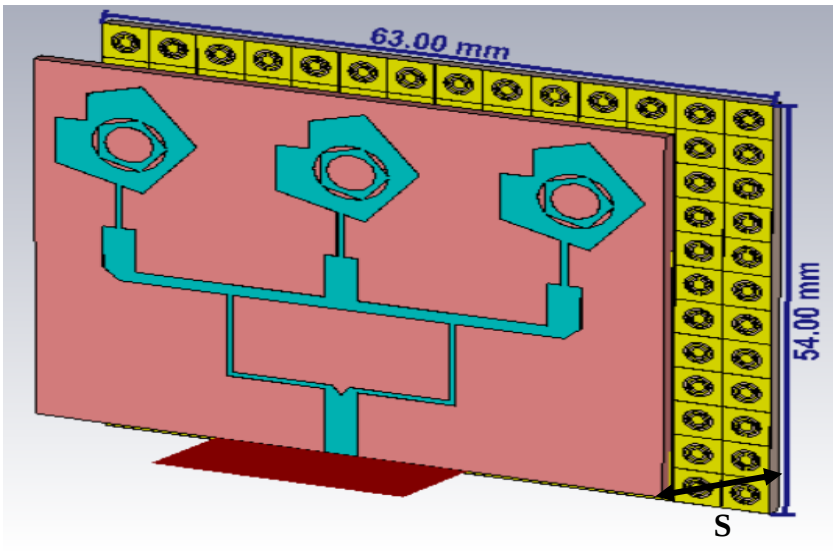

a)

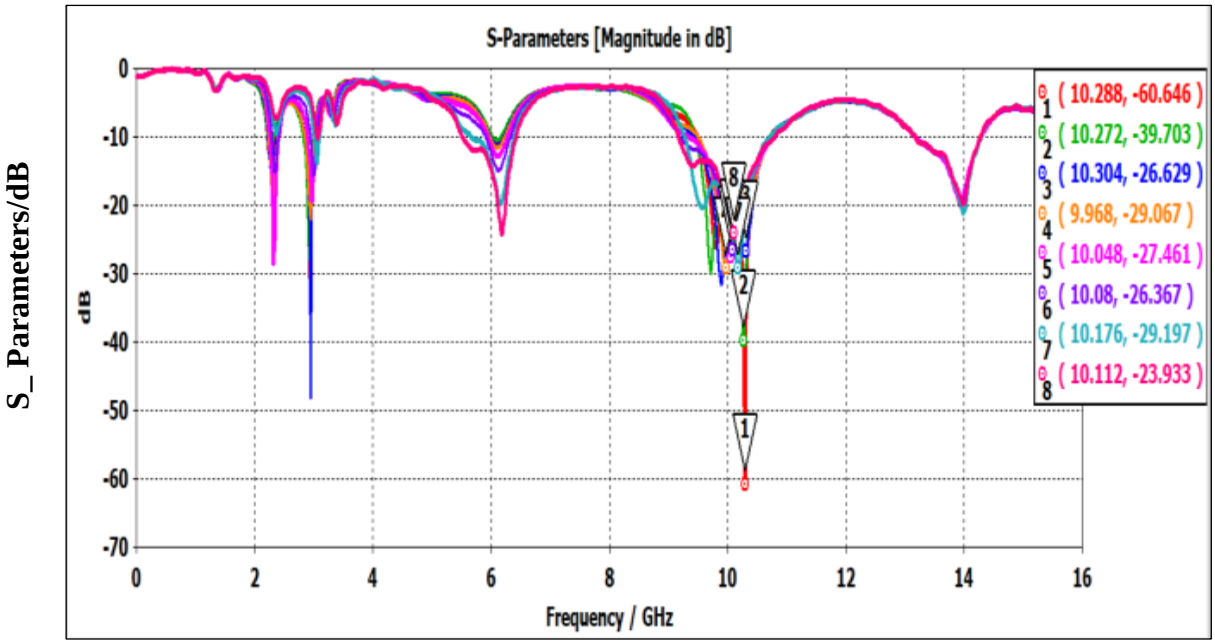

b)

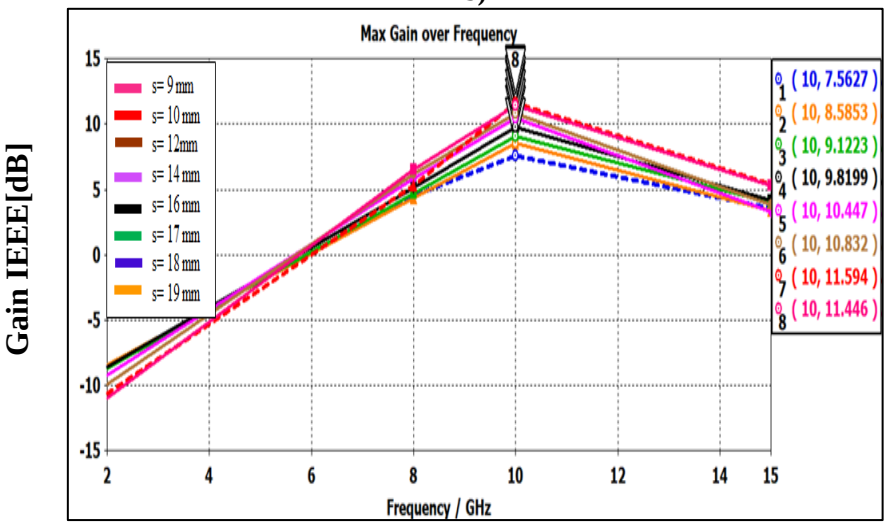

c)

Figure 16. a) Perspective view of the embedded 1×3 antenna array with MTM Superstrate layer **b)** Analysis of S11 parameters at various distances at 10 GHz, **c)** The gain parametrically at different distances at 10 GHz

Table 9: Return losses & gain of 1×3 antenna array with the reflector for different spacing

Spacing between 1×3 antenna array and MTM superstrate layer (S)mm	Return Losses S_{11} (dB)	Gain (dBi)
9	-23.85	11.44
10	-29.19	11.6
12	-26.36	10.83
14	-27.44	10.44
16	-29.06	9.81
17	-26.59,-31.39	8.81,9.1
18	-60.64	7.56
19	-39.70	8.58

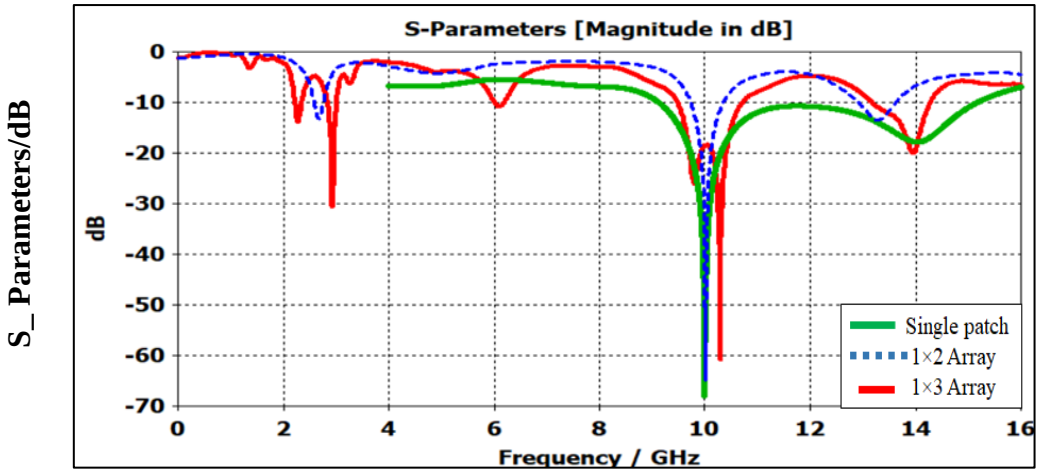

a)

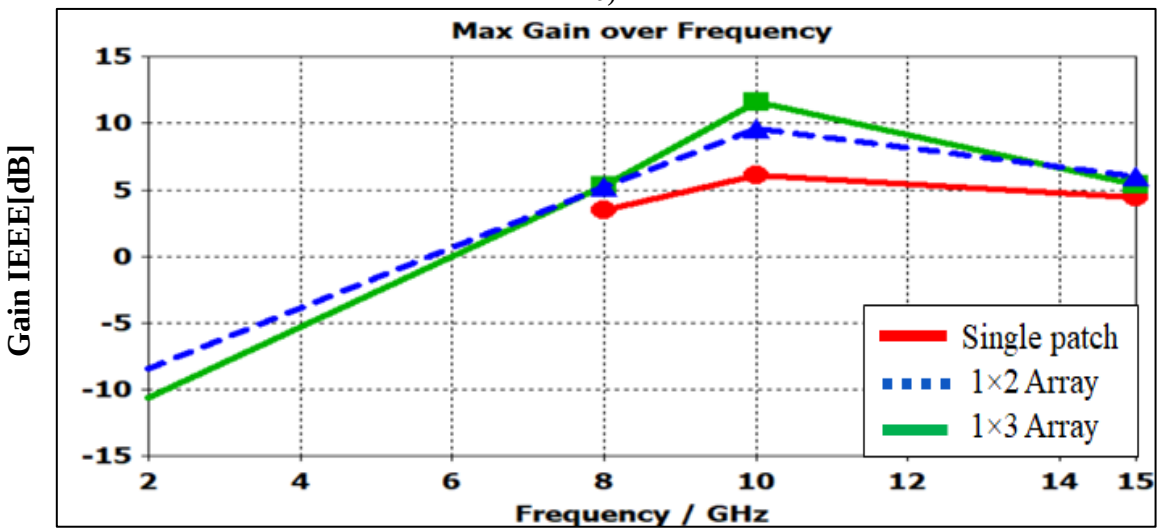

b)

Figure 17(a) Comparing the S-parameters of one, two, and three elements with the MTM superstrate layer b) Comparing the gain of one, two, and three elements with the MTM superstrate layer

5.2. Findings regarding radiation pattern and efficiency

When the 1×2 antenna array with a superstrate layer is used at 10 GHz, the simulated gain is 9.58 dBi, the directivity is 12.4 dBi, and the radiation efficiency is 79.11%. In comparison, the 1×3 antenna array with a superstrate layer at 10 GHz achieves a gain of 11.6 dBi, a directivity of 14.3 dBi, and maintains the same radiation efficiency of 79.11%. The greater losses introduced by the MTM array cells contribute to the decreased radiation efficiency. However, metamaterials, synthetic materials with characteristics not found in naturally occurring materials, offer unique advantages such as improved directivity and radiation pattern control.

While these materials can introduce additional losses, particularly in absorption and scattering, their potential to enhance antenna array performance is significant. When placed as a superstrate layer on the antenna array, metamaterials absorb some of the incident electromagnetic energy and disperse the radiated energy in different directions away from the desired direction. This results in a loss of radiated power and a decrease in the overall efficiency of the antenna array system.

The normalized radiation patterns for single, 1×2, and 1×3-element antenna arrays are provided for the broadside. The H-plane ($\varphi = 90°$) directivity of the single-band antennas at 10 GHz, shown in Figure 18, indicates a main lobe intensity of -1.8 dBi oriented at 55 degrees. These results clearly show the good performance of the simulated single-band antenna, which has a nearly isotropic radiation pattern with side lobe levels of -3.2 dB at 10 GHz.

The H-plane (φ = 90°) directivity of the proposed 1×2 corporate-fed antenna with an MTM layer is illustrated in Fig. 19. There is a noticeable increase in the size of the main lobe compared to the single-band antenna, with a directivity of 12.4 dBi, a main lobe direction of 4°, and a half-power beamwidth (HPBW) of 35.6°. Correspondingly, side lobe levels decrease by -9.9 dB, as observed from the directivity polar plot. Fig. 20 displays the H-plane (φ = 90°) directivity of the proposed 1×3 corporate-fed antenna with an MTM layer. The main lobe magnitude increases slightly to 14.3 dBi, while the side lobe levels remain nearly the same as the 1×2 antenna array at -9.9 dB.

While our research shows promising results, it also highlights some challenges. The E-plane (φ = 0°) directivity of the single patches is given in Fig. 21, showing a slight increase in the main lobe magnitude by 0.712 dB. The main lobe direction decreases to 42°, with an HPBW of 70.7° and side lobe levels of -1.6 dB at 10 GHz. For the 1×2 corporate-fed pentagonal arrays, a main lobe magnitude of 12.3 dBi and an HPBW of 38.8° were obtained, with side lobe levels of -15.5 dB, as shown in Fig. 22. The directivity polar plot in the E-plane (φ = 0°) for the 1×3 corporate-fed pentagonal arrays indicates a maximum magnitude of 10.8 dBi, side lobe levels of -14.2 dB, and a HPBW of 26.1°, as presented in Fig. 23. These findings underscore the need for further investigation and development to fully understand and mitigate the challenges posed by metamaterials in antenna array design.

From the above analysis, it is evident that the side lobes distort the radiation pattern. However, the MTM reflector layer's capacity to absorb diffracted waves from the antenna array's partial ground plane allows it to maintain high gain. In the suggested array, the MTM superstrate layer cuts down on back radiation (side lobes) by a large amount across the whole frequency range of operation. This demonstrates the high directivity that the MTM array cells achieved. The IEEE 3-D gain of the single-band antenna, as designed in Section 2.1, is shown in Fig. 24. The single patch achieved gains of 6.07 dB at 10 GHz. Figure 25 displays a 1×2 corporate-fed pentagonal array with an MTM substrate layer. It also displays its IEEE 3-D gain of 9.59 dB at 10 GHz. Figure 26 shows that the 1×3 corporate-fed array with the MTM superstrate layer gained 11.6 dB at the same operating frequency. This was a big improvement over the single-band patches and 1×2 antenna arrays that were made before. The results of the studied design antennas are compared across different configurations: single patch, 1×2, and 1×3 element array antennas, both with and without MTM superstrate layers. This comparison is presented in Table 10. This new 1×3 corporate-fed pentagonal array works better at 10 GHz regarding side lobe level, gain, directivity, and input reflection coefficient. Specifically, it surpasses all other designed antennas in terms of gain and directivity (H-field and E-field). However, the bandwidth performance needs improvement compared to the single-patch antenna, which exhibits significantly better bandwidth.

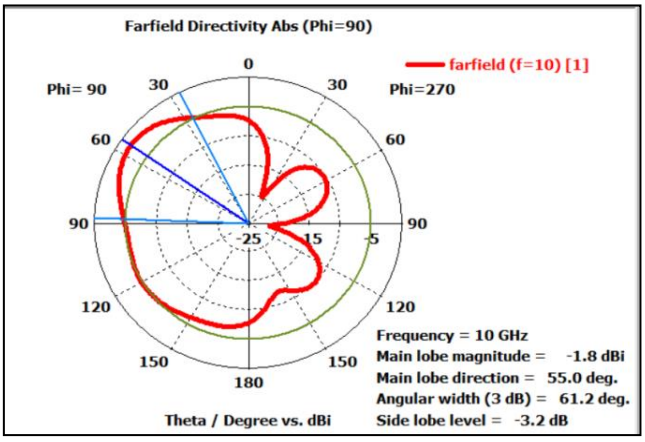

Figure 18. Directivity of single patch antennas at 10 GHz in H-plane (φ = 90°)

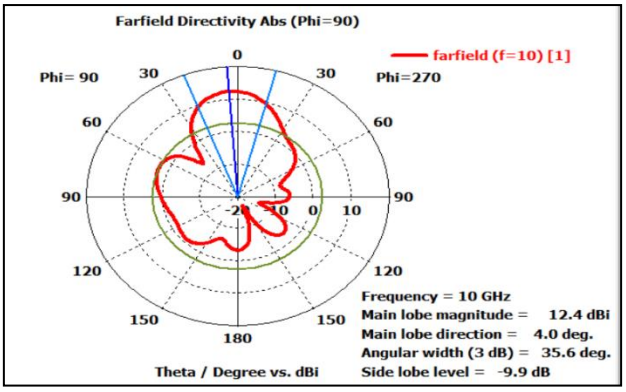

Figure 19. Directivity of 1×2 array antennas at10GHz in H-plane (φ = 90°)

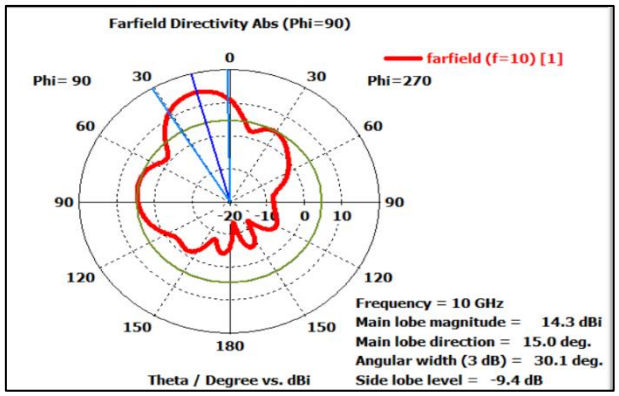

Figure 20. Directivity of 1×3 array antennas at10 GHz in H-plane (φ = 90°)

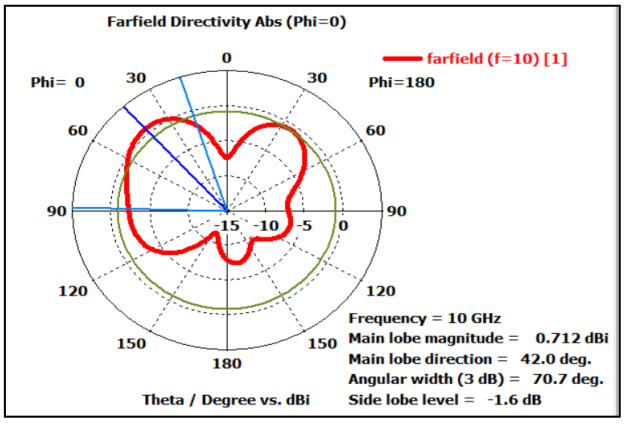

Figure 21. Directivity of single patch antennas at 10 GHz in E-plane (φ = 0°)

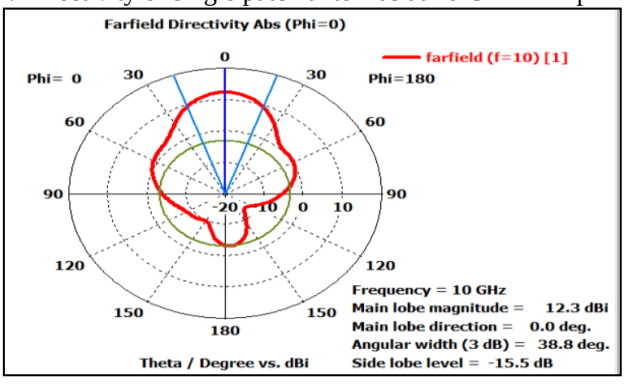

Figure 22. Directivity of 1×2 array antennas at10 GHz in E-plane (φ = 0°)

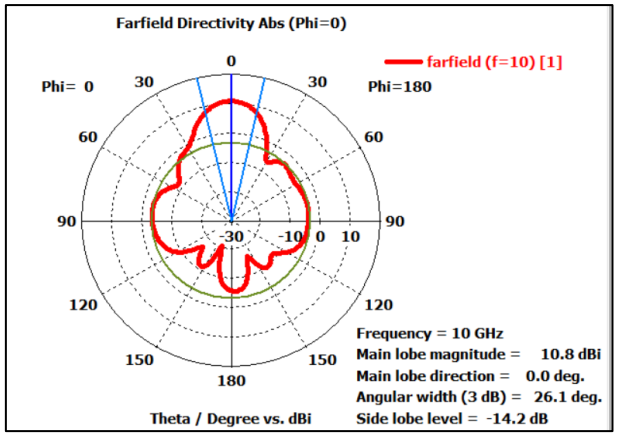

Figure 23. Directivity of 1×3 array antennas at10 GHz in E-plane (φ = 0°)

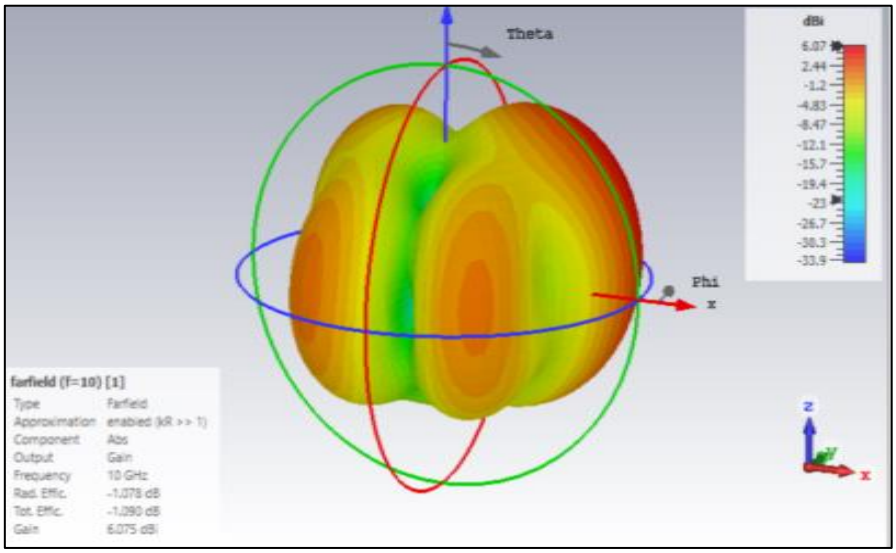

Figure 24. Gain of single-band antenna at10 GHz

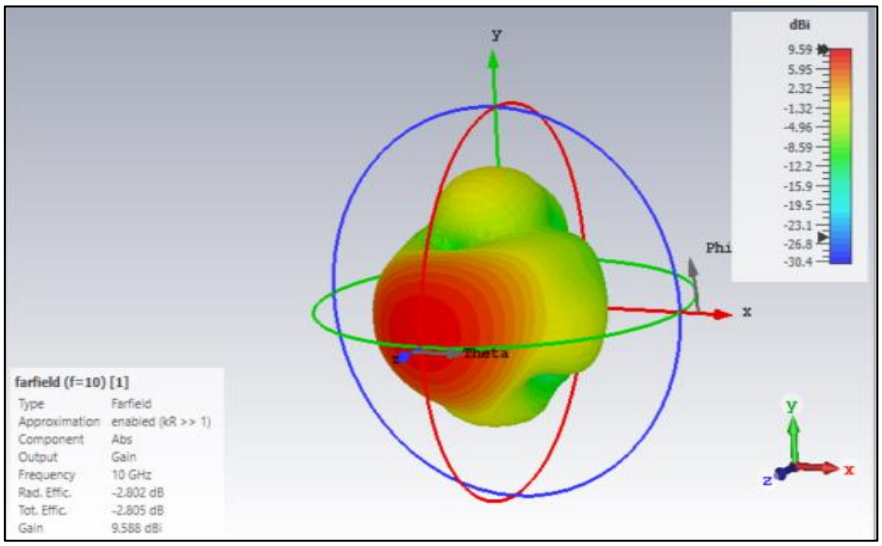

Figure 25. Gain of proposed 1×2 antenna array at 10 GHz

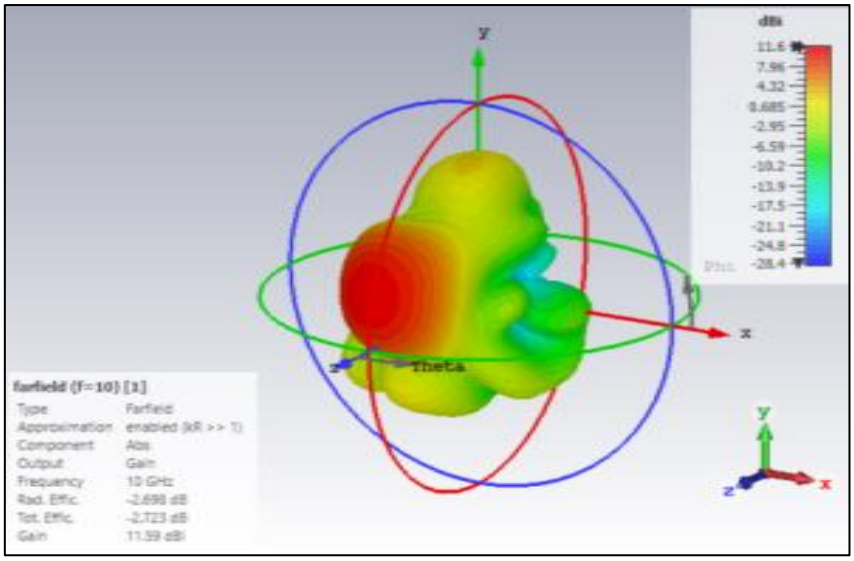

Figure 26. Gain of proposed 1 × 3 antenna array at 10 GHz

Table 10: Comparative study of proposed work with existing designs

Antenna Type	Resonant Freq (GHz)	Return Loss (dB)	Gain (dB)	Directivity (dB)	Bandwidth (MHz)	Side lobes level (SLL)
Single Patch Antenna	10 GHz	-67.87	6.109	7.15	6016	-3.2
1×2 antenna Array without MTM superstrate layer	10 GHz	-48.6	7.52	10.62	595.5	-6.1
1×2 antenna Array with MTM Superstrate layer	10 GHz	-64.86	9.588	12.3	602	-15.5
1×3 antenna Array without MTM Superstrate layer	10 GHz	-57.46	9.69	12.4	1269	-5.8
1×3 antenna Array With MTM Superstrate layer	10 GHz	-60.64	11.6	14.3	1283	-14.2

6. Simulation and measurement results

The two-element antenna array with an MTM superstrate layer was manufactured using an economical FR-4 substrate at the Ministry of Science and Technology. Figure 27 (a, b) displays the constructed prototype of the antenna array. Figure 27(c) shows spacers made of insulating tapes to support the array antenna and MTM reflector layer, which were observed to have no significant impact on the antenna's performance. The testing environment maintained stable temperature and humidity conditions to minimize external environmental impacts on performance. The MS4642A VNA (Vector Network Analyzer), which works between 300 MHz and 20 GHz, was used to take S11 measurements at 10 GHz to ensure the simulations were accurate. The simulated and measured S11 characteristics, both with and without a reflector layer, are presented in Figure 28 (a, b). Several factors, such as fabrication conditions, environmental changes during measurements, and variations in the thickness of the insulating material (FR-4), affected discrepancies between the simulated and measured results. Notably, there was a significant disparity between the results, primarily because the simulated substrate was 1.4 mm thick while the actual manufactured substrate had a thickness of 1.5 mm.

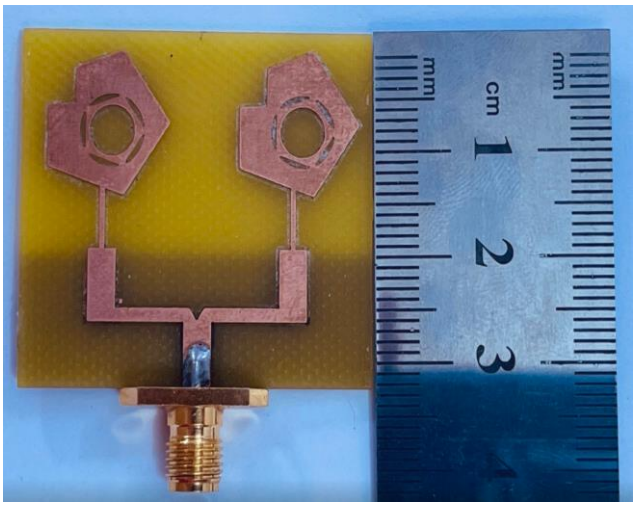

a)

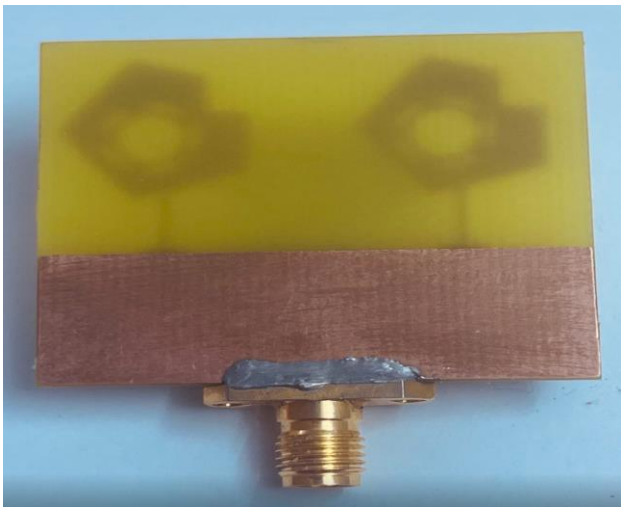

b)

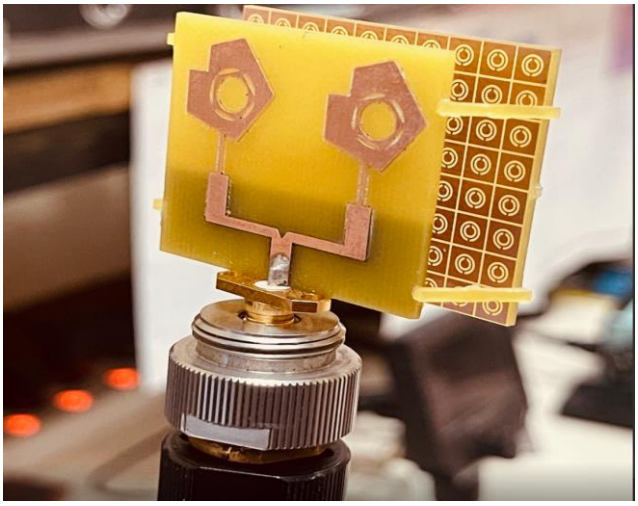

(c)

Figure 27. Prototype fabricated of the 1 × 2 antenna array (a) Front view, (b) Back view, (c) Integration of the MTM superstrate layer and array antenna.

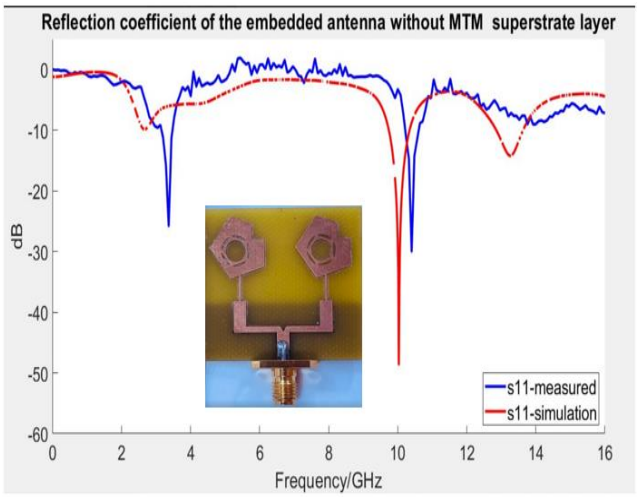

a)

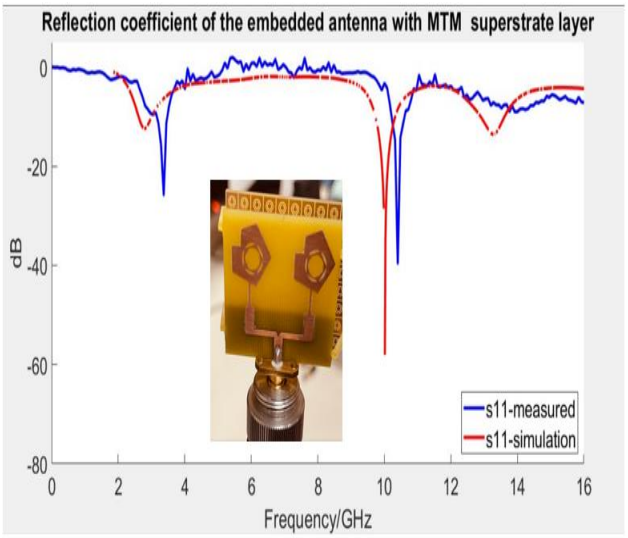

b)

Figure 28. a) The simulated and measured S11 characteristics without the MTM superstrate layer b) The simulated and measured S11 characteristics with the MTM superstrate layer

This study encountered several challenges and limitations during the design of the integrated antenna array. These theoretical and practical issues must be addressed to ensure the successful implementation of the super-material substrate in real-world applications. The most notable challenges include:

1. Fabrication Precision and Cost: The intricate design of the superstrate necessitates high precision, which can render fabrication costly and technically challenging, especially for mass production. To mitigate these issues, exploring advanced manufacturing techniques and materials that offer improved precision and cost-effectiveness could be beneficial.
2. Integration Complexity: The proper alignment of the superstrate with the pentagonal microstrip patch antennas is not just a technical challenge but a complex task crucial for achieving optimal performance.
3. Material and Structural Stability: The lack of a full ground plane presents structural challenges, impacting durability and reliability under various conditions.
4. Environmental Sensitivity: It is vital to ensure reliable performance in diverse environmental conditions, such as variations in temperature, moisture, and

stress, especially in military and aerospace applications.

5. Optimization for Frequencies: Although significant gains have been achieved at 10 GHz, optimizing performance across the entire X-band frequency range introduces additional complexity.
6. Economic Feasibility: Achieving commercial viability is not just a goal but a necessity that requires balancing the high costs of advanced materials and complex manufacturing processes with the benefits of performance gains.

The proposed antenna array design utilizing the MTM superstrate technique demonstrates significant advancements over previous studies [30–38], as shown in Table 11. Key improvements are highlighted at several points, including:

1. Broad Operating Bandwidth: The proposed 1×3 element array antenna showcases an operating bandwidth of 1283 MHz. This is substantially higher than earlier designs, such as the 40 MHz bandwidth of Ref. [32] and the 500 MHz bandwidth of Ref. [36], indicating superior broadband capability.
2. Enhanced Gain: The proposed design, the pinnacle of innovation, achieves a peak gain of 11.6 dBi, surpassing earlier works like 8.25 dBi from Ref. [33] and 10.1 dBi from Ref. [38]. The integration of the MTM superstrate, a testament to its superiority, significantly improves the antenna's radiation characteristics, contributing to this higher gain.
3. Better Return Losses: The proposed design has better impedance matching and less signal reflection than previous studies, with return losses of -60.64 dB for the 1x3 array compared to -43.856 dB in Ref. [31] and around -48.6 dB in Ref. [34].
4. Enhanced Efficiency: Compared to the 58% efficiency reported by Ref. [33], the proposed design's efficiency of roughly 79.11% represents a significant performance improvement.
5. Compact and Effective Design: Despite its compact size, the proposed antenna array maintains high performance across essential metrics, substantially advancing over previous designs.

Overall, the proposed antenna array design presents a significant advancement over previous performance improvements by employing excellent return losses and improved efficiency significantly advance over previous designs. These enhancements make it highly suitable for applications within the X-band frequency range, commonly used in radar and satellite communication systems. This particular frequency enables optimal performance in these applications due to its balance between range and resolution, making it highly suitable for civilian and military technologies. Although the current design is optimized for narrowband performance at this frequency, we recognize the value of expanding the bandwidth to cover the entire X-band with consistent gain. We are exploring design modifications to broaden the bandwidth while maintaining high performance, aiming to enhance the antenna's versatility across various applications.

Table 11: A Comparison between the proposed structure and previously reported designs

Ref.	No. of Array Elements	Size (mm^2)	Suggested Decoupling technique	Operating Frequency (GHz)	Return losses S_{11}(dB)	Efficiency η (%)	Bandwidth (MHz/GHz)	Gain value (dBi)
30 2017	Single element 1× 2 $Array$ 1× 4 $Array$	----------	Corporate Feeding	10 GHz	-30.37	NL	NL	11.57
31 2018	Single element 1× 2 $Array$	120×60	EBGTL	9.46GHz	-43.856	NL	5.28 GHz	9.69

32	Single element	----------	DGS	9.1 GHz	- 14.93	69.53	40 MHz	10.38
2018	1× 4 *Array*							
33	Single element	26 ×30	MTM &TCM	10 GHz	-25	58	906 MHz	5.36
2019	1× 2 *Array*	35×28	Series feed	10 GHz	-38			8.25
34	Single element	44×16	Corporate feed	28 GHz	-20.7	NL	28.01 GHz	7.98
	1× 2 *Array*	36×74		27.58 GHz	-32.9			8.85
2020	1× 4 *Array*	35×37	Corporate-series feed	27.96 GHz	-48.6			9.49
35	Single element	66×58	DGS	2.54 GHz	-16	NL	187.5 MHz	3.5
2021	1× 4 *Array*	280×65		2.43GHz	-13			10
36	Single element	42×43.05	Metamaterial	2.4 GHz	-26	NL	500 MHz	3.223
2021	1× 3 *Array*	126 × 43.05	Superstrate	2.4 GHz	-14			8.1667
37	Single element	52×62	corporate-series fed	2.2GHz	-22	NL	90 MHz	3.38
	1× 2 *Array*	114.2×62		2.2GHz	-25.9		110 MHz	5.52
2023	1× 4 *Array*	254.2×62		2.2GHz	-15.3		180 MHz	7.84
38	Single element	47.57×39	corporate-series fed	2.4 GHz	-26.39	86	33.06 MHz	4.85
	1× 2 *Array*	.12		2.4 GHz	-22.90			10.1
2024	1× 4 *Array*	160×70		2.4 GHz	-31.90		50.41MHz	11.5
Proposed work	**Single element**	**35 × 23**		**10 GHz**	**-67.78**			**6.07**
	1× 2 Array	**38.5 × 34.1**	**Metamaterial**	**10 GHz**	**-64.86**	**79.11**	**6016 MHz**	**9.588**
	1× 3 Array	**59.05 × 48.3**	**Superstrate**	**10 GHz**	**-60.64**		**1283 MHz**	**11.6**

7. Conclusions

This research conclusively shows that metamaterial superstrates can effectively mitigate mutual coupling in compact antenna arrays, a challenge magnified by the miniaturization of modern communication systems. We achieved significant performance improvements by employing a pentagonal.

Microstrip patch antennas at 10 GHz within the X-band frequency range using a superstrate with nested open circular rings. A grid of 14×12 cells on a substrate without a full ground plane greatly improves antenna performance, especially in a 1×3 array. It demonstrates a marked increase in gain over single and two-element arrays and shows better impedance matching through improved input reflection coefficients. These enhancements reduce pattern distortion, impedance mismatch, and operational in efficiencies often seen in phased arrays. This study provides crucial insights into antenna array interactions and offers valuable design strategies for high-gain, compact antenna arrays, advancing more efficient and robust X-band communication systems.

References

[1] P. A. Nageswara Rao, Y. Sukanya, and C. Manohar Kumar, "Design and Performance of Π-Shape Slotted Microstrip Patch Antenna Arrays," in 2022 International Conference on Breakthrough in Heuristics And Reciprocation of Advanced Technologies (BHARAT), Visakhapatnam, India, 2022, pp. 83-88. doi: 10.1109/BHARAT53139.2022.00027.

[2] L. L-Y and Z-H. Tu, "Low-profile and broadband microstrip antenna with pattern diversity," Microw. Opt. Technol. Lett., vol. 65, pp. 2988-2994, 2023. doi: 10.1002/mop.33819.

[3] Y. Liu and H. Liu, "Target Height Measurement under Complex Multipath Interferences without Exact Knowledge on the Propagation Environment," Remote Sens., vol. 14, no. 13, 2022, Art. no. 33099. doi: 10.3390/rs14133099.

[4] A. Akinyele et al., "Investigation of Small-Scale and Multipath Fading of Radio Wave Propagation in a Complex Building Environment," Int. J. Commun. Antenna Propag., vol. 12, no. 6, 2022, Art. no. 21849. doi: 10.15866/icecap.v12i6.21849.

[5] R. B. Nassir and A. K. Jassim, "Design of mimo antenna for wireless communication applications," J. Eng. Sustain. Dev., vol. 26, no. 4, pp. 36–43, 2022.

[6] D. M. Pozar, Microwave Engineering, 4th ed. Wiley, 2011.

[7] G. Matthaei, L. Young, and E. M. T. Jones, Microwave Filters, Impedance-Matching Networks, and Coupling Structures. Artech House, 1980.

[8] S. R. Best, Microstrip and Printed Antennas: New Trends, Techniques and Applications. Wiley, 2011.

[9] A. T. Alphones, Design of Microstrip Patch Antennas. Artech House, 2011.

[10] K. J. Vinoy and J. G. Malherbe, Analysis and Design of Multilayered Microstrip Antennas for Wireless Applications. Artech House, 2000.

[11] N. Yan, D. Song, Y. Luo, and K. Ma, "A sequentially rotated feeding circularly polarized stacked patch antenna array based on SISL," Wiley J., vol. 65, no. 1, pp. 256-263, Jan. 2023.

[12] A. K. Nghaimesh and A. K. Jassim, "Triple-band circular patch microstrip antenna for wireless communication," J. Eng. Sustain. Dev., vol. 28, no. 1, pp. 64–74, 2024.

[13] M. Bahare et al., "Mutual coupling reduction in microstrip array antenna by employing cut side patches and EBG structures," Prog. Electromagn. Res. M, 2020. doi: 10.2528/PIERM19100703.

[14] Y. He et al., "Wideband decoupling technique for two-element antenna array using pixel neutralization line," Microw. Opt. Technol. Lett., vol. 64, no. 4, pp. 33363, 2022. doi: 10.1002/mop.33363.

[15] A. Khalid, Jassim, R. H. Thaher, "Enhancement gain of broadband elliptical microstrip patch array antenna with mutual coupling for wireless communication," Indones. J. Electr. Eng. Comput. Sci., vol. 13, no. 1, pp. 217-225, Jan. 2019. doi: 10.11591/IJEECS.v13.i1.pp217-225.

[16] A. Rashidifar and K. E. Drenkhahn, "Reduction of Mutual Coupling between Dual-Polarized Antenna Elements Using Defected Ground Structures," in Proc. 17th European Conf. on Antennas and Propagation (EuCAP), Florence, Italy, 2023, pp. 1-5. doi: 10.23919/EuCAP57121.2023.1013363.

[17] W. Chang et al., "Mutual coupling reduction in antenna arrays using the novel mushroom electromagnetic band gap and defected ground structure," Microw. Opt. Technol. Lett., vol. 66, 2024, Art. no. e34084. Doi: 10.1002/mop.34084.

[18] S. Barman et al., "Gain and Directivity enhancement of microstrip patch antenna using metamaterial superstrate containing rectangular split ring resonators," 2023. doi: 10.21203/rs.3.rs-1421742/v1.

[19] P. K. Gupta, "A Microstrip Antenna Using I-Shaped Metamaterial Superstrate with Enhanced Gain for Multiband Wireless Systems," Micromachines, vol. 14, no. 2, 2023, Art. no. 0412. doi: 10.3390/mi14020412.

[20] R. Mahdi Salih and A. K. Jassim, "Microstrip patch antenna with metamaterial using superstrate technique for wireless communication," Bull. Electr. Eng. Inform., vol. 10, no. 4, pp. 2722, 2021. doi: 10.11591/EEI.V10I4.2722.

[21] C. Arora, S. S. Pattnaik, and R. N. Baral, "Metamaterial inspired DNG superstrate for performance improvement of microstrip patch antenna array," Int. J. Microwave Wireless Technol., vol. 10, no. 3, pp. 318-327, 2018. doi: 10.1017/S1759078717001428.

[22] H. Alwareth et al., "A Wideband High-Gain Microstrip Array Antenna Integrated with Frequency-Selective Surface for Sub-6 GHz 5G Applications," Micromachines, vol. 13, 1215, 2022. Available: https://doi.org/10.3390/mi13081215.

[23] F. Ouberri, A. Tajmouati, N. Chahboun, L. El Abdellaoui, and M. Latrach, "A novel wideband circularly-polarized microstrip antenna array based on DGS for wireless power transmission," Telkomnika, vol. 20, no. 3, pp. 485–493, Jun. 2022. doi: 10.12928/TELKOMNIKA.v20i3.21711

[24] C. A. Balanis, Antenna Theory: Analysis and Design, 3rd ed. John Wiley & Sons, Wiley-Interscience, 2015.

[25] B. Olatujoye and J. C. Saturday, "Design and Performance Analysis of 4-Element Multiband Circular Microstrip Antenna Array for Wireless Communications," IOSR J. Electron. Commun. Eng., vol. 18, no. 1, Ser. I, pp. 01-07, Jan.–Feb. 2023. DOI 10.9790/2834-1801010107.

[26] S. Lou, S. Qian, and W. Wang, "Influence of Random Errors in Element Positions on Performance of Antenna Arrays Considering Mutual Coupling Effect," IEEE Antennas Wireless Propag. Lett., 2023. doi: 10.1109/LAWP.2023.3281569.

[27] O. Ifeanyi F., K. M. Udofia, and K. M. Udofia, "Comparative Analysis of Microstrip Antenna Arrays with Diverse Feeding Techniques," J. Eng. Res. Rep., vol. 26, no. 1, pp. 18-38, 2024. Article no. JERR.111205. ISSN: 2582-2926. DOI: 10.9734/JERR/2024/v26i11060.

[28] M. Sohail, "Near field focusing of rectangular microstrip patch antenna array," February 2016.

[29] B. Olatujoye and J. C. Saturday, "Design and performance analysis of 4-element multiband circular

microstrip antenna array for wireless communications," IOSR J. Electron. Commun. Eng., vol. 18, no. 1, pp. 1-7, 2023.

[30] R. N. Leela, "1×4 Rectangular Patch Array Operating at 10GHz Using Corporate Feeding Technique," Int. J. Eng. Dev. Res., vol. 5, no. 2, 2017. ISSN: 2321-9939. Available at: www.ijedr.org.

[31] H. S. Gally, Z. A. Ahmed, and A. H. Abood, "Mutual Coupling Reduction In Microstrip Antenna Array Using Ebg," J. Basrah Res. Sci., vol. 44, no. 1A, 2018. Available: http://brsj.cepsbasra.edu.iq/.

[32] V. N. Lakshmana Kumar, M. Satyanarayana, and S. P. Singh, "A Novel Technique for Sidelobe and Backlobe Reduction in Rectangular Microstrip Antenna Array Using Defected Ground Structures," Int. J. Appl. Eng. Res., vol. 13, no. 22, pp. 15961-15966, 2018.

[33] E. K. I. Hamad and A. Abdelaziz, "Performance of a Metamaterial-based 1×2 Microstrip Patch Antenna Array for Wireless Communications Examined by Characteristic Mode Analysis," Electromagnetics, Radio Eng., vol. 28, no. 4, Dec. 2019. doi: 10.13164/re.2019.0680.

[34] J. Maharjan and D.-Y. Choi, "Four-Element Microstrip Patch Array Antenna with Corporate-Series Feed Network for 5G Communication," Hindawi Int. J. Antennas Propag., 2020, Art. ID 8760297. Available: https://doi.org/10.1155/2020/8760297.

[35] S. Dharmpatre and M. Sutaone, "Design and Characterization Analysis of Microstrip Patch Array Antenna with Dumbbell-shaped DGS for ISM Band Applications," Turk. J. Comput. Math. Educ., vol. 12, no. 9, pp. 2652–2663, 2021.

[36] S. Kumar D and S. Suganthi, "Novel hybrid metamaterial to improve the performance of a beamforming antenna," J. Phys. Conf. Ser., vol. 1921, 2021, Art. no. 012020. Doi: 10.1088/1742-6596/1921/1/012020.

[37] A. D. Santoso, F. B. Cahyono, H. B. Bagus, and M. H. Saleh, "Parametric Study of Rectangular Microstrip Array Antenna at 2.2 GH," in Proc. 2023 Int. Conf. on Advance Transportation, Engineering, pp. 154–167. doi: 10.2991/978-94-6463-092-3_14.

[38] O. I. F. Udofia, K. M. Udofia, and K. M. Udofia, "Comparative Analysis of Microstrip Antenna Arrays with Diverse Feeding Techniques," J. Eng. Res. Rep., vol. 26, no. 1, pp. 18-38, 2024. Article no. JERR.111205. ISSN: 2582-2926.